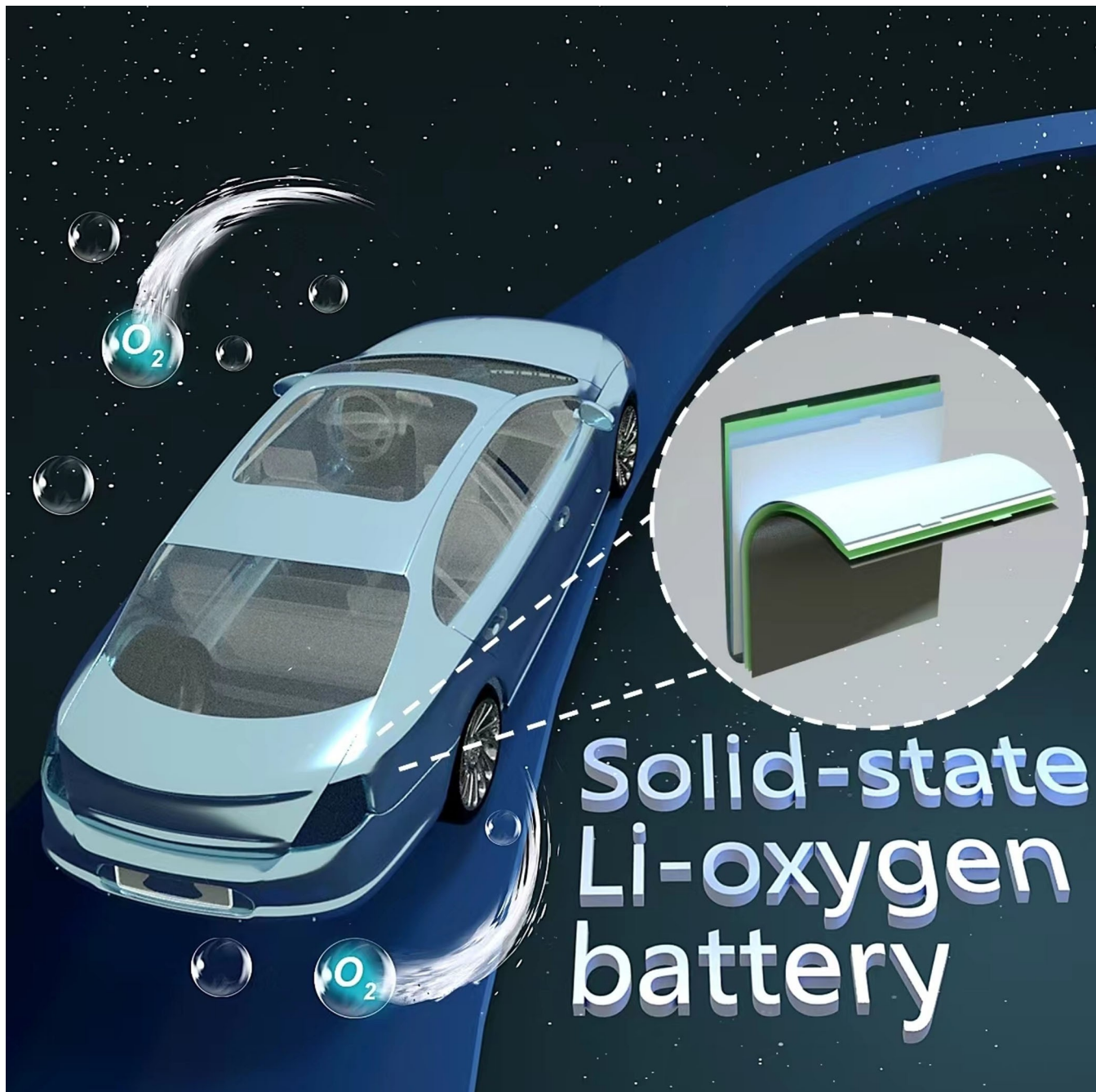


Special
Collection

Constructing Rechargeable Solid-State Lithium-Oxygen Batteries

Minghui Li⁺^[a] Kecheng Pan⁺^[a] Weicheng Wang,^[a] Shuochao Xing,^[a] Yaying Dou,^[a, b] Zhang Zhang,^{*[a, b]} and Zhen Zhou^{*[a]}



Lithium-oxygen batteries (LOBs) hold great potential for electrochemical energy storage due to their high theoretical energy density. However, the utilization of conventional liquid electrolytes raises safety concerns such as flammability and leakage, which are also problematic in lithium-ion batteries. The development of practical open battery systems employing volatile liquid electrolytes, with the ultimate goal of lithium-air batteries, presents particular challenges. Solid-state electrolytes (SSEs) have emerged as a promising solution to tackle these issues. In the past two decades, SSEs have garnered significant

attention and have been successfully implemented in LOBs. This review aims to highlight recent advancements in SSEs for LOBs, exploring the opportunities and challenges associated with developing SSEs possessing high ionic conductivity, interfacial compatibility, and stability. The objective is to enhance reversibility, promote an increase in stable triple-phase boundaries, and safeguard the Li anode in open battery systems. Finally, we put forth future directions for the advancement of solid-state Li-air batteries.

1. Introduction

The increasing global demand for energy, combined with the depletion of fossil fuels, has emphasized the importance of developing eco-friendly and renewable energy technologies. Fossil fuel combustion generates hazardous gas pollution, creating an urgent need for cleaner energy solutions.^[1] To maximize the use of sustainable clean energy, researchers are increasingly focusing on battery development.^[2] Though lithium-ion batteries (LIBs) have been widely used, they cannot fully meet the high energy density demand for electric vehicles.^[3,4] This has led to the exploration of lithium-oxygen batteries (LOBs), which have the potential to achieve an ultrahigh theoretical energy density of approximately 3500 Wh kg⁻¹, comparable to gasoline.^[5] LOBs offer promising prospects for the future of electric vehicles, and would greatly enhance their driving range.^[6]

Although the theoretical specific energy of rechargeable LOBs is 5–10 times as high as that of LIBs,^[7] critical challenges in terms of low capacity and poor cycle life limit further development of LOBs into a practical technology.^[8] A typical rechargeable LOB is composed of a Li anode, a Li⁺ conducting electrolyte, a separator, and a cathode.^[9] Traditional LOBs mainly use liquid electrolytes (LEs). However, as an important component in the battery, the LE often encounters several serious challenges concerning safety issues, volatilization,

leakage and flammability at high temperatures.^[10] Also, the rate of oxygen transporting from the cathode to reaction sites is an important factor on battery performances such as discharge capacity, rate capability, round-trip efficiency and cycling stability.^[11] In addition, lithium dendrites can puncture through the electrolyte and contact the cathode, causing short circuit and even explosion.^[12]

As shown in Figure 1, solid-state electrolytes (SSEs) have emerged as a promising alternative for the LE and separator to overcome the challenges associated with LEs in LOBs.^[13] Firstly, SSEs can eliminate safety concerns related to electrolyte leakage and flammability. Secondly, SSEs can facilitate the development of practical open battery systems, ultimately leading to the realization of Li-air batteries. Lastly, SSEs with high hardness can resist lithium dendrite penetration, and the solid electrolyte film can serve as a protective barrier to safeguard the Li anode from active species, such as O₂ and H₂O, which may diffuse from the cathode. Thus, the use of SSEs significantly improves the reliability and stability of LOBs, with wider electrochemical window, greater thermal stability, and higher Li⁺ transference number. Certainly, in the future, environmental friendliness and easy preparation in technology need to be considered.

Although SSEs offer several advantages, they also have intrinsic limitations that hinder their practical application. One of the main challenges is their relatively low ionic conductivity compared with LEs, underscoring the need for developing SSEs with distinct ion conduction pathways that can enhance their conductivity. Additionally, there is significant resistance at the interface between SSEs and electrodes, which limits their further use in LOBs. Finally, the discontinuity of the electron conduction path, Li⁺ conduction path, and O₂ diffusion path in solid-state LOBs (SSLOBs) directly impact the formation and decomposition of discharge products. These challenges must be addressed to enable the practical implementation of SSEs in LOBs.

This review provides a comprehensive analysis of various types of SSEs used in LOBs, including their internal compositions, Li⁺ conduction paths, and reaction mechanisms. By examining these factors, we aim to identify appropriate strategies for developing high-performance batteries. We also analyze the challenges associated with SSEs, such as interface issues resulting from direct contact between SSEs and electrodes. To address these challenges, we summarize optimization methods for the solid-solid interface, which can reduce interface

[a] M. Li,[†] Dr. K. Pan,[†] W. Wang, S. Xing, Dr. Y. Dou, Dr. Z. Zhang, Prof. Z. Zhou
Interdisciplinary Research Center for Sustainable Energy Science and
Engineering (IRC4SE2), Engineering Research Center of Advanced Functional
Material Manufacturing of Ministry of Education, School of Chemical
Engineering
Zhengzhou University
Zhengzhou 450001, P.R. China
E-mail: zhangzhang199001@zzu.edu.cn
zhenzhou@zzu.edu.cn

[b] Dr. Y. Dou, Dr. Z. Zhang
Key Laboratory of Advanced Energy Materials Chemistry (Ministry of
Education), College of Chemistry
Nankai University
Tianjin 300071, P.R. China

[†] These authors contributed equally to this work.

Supporting information for this article is available on the WWW under
<https://doi.org/10.1002/batt.202300230>

An invited contribution to a Special Collection on Young Scientists in Battery
Research.

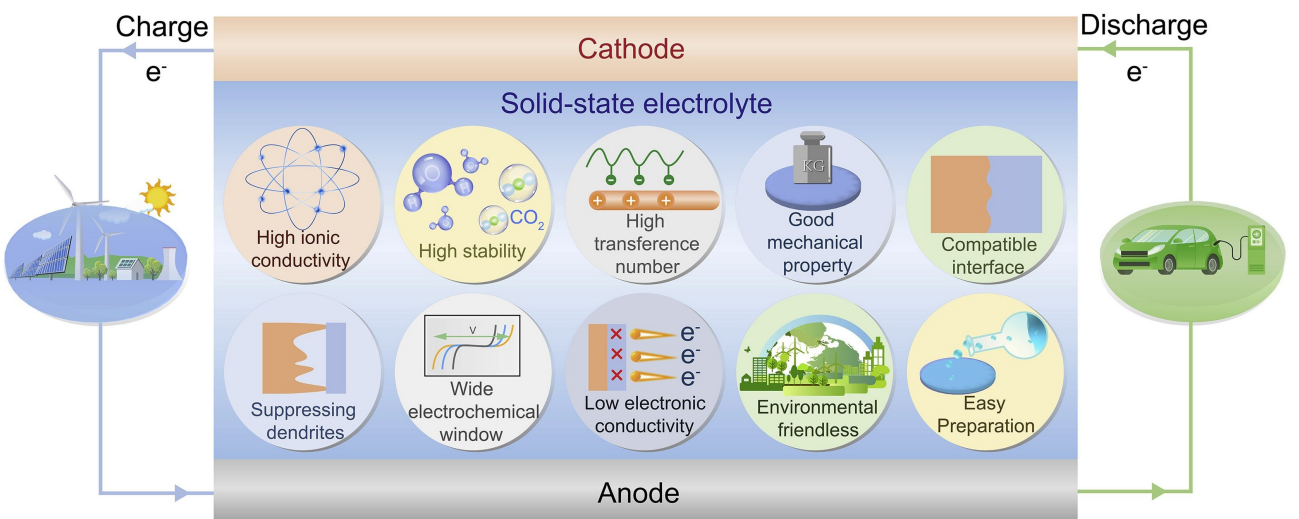


Figure 1. Requirements for SSEs in high-energy LOBs. Reprinted from Ref. [14] with permission. Copyright (2023) Elsevier.

resistance and enhance interface compatibility. Finally, we discuss the potential extension of SSEs to other Li-air batteries

and offer meaningful suggestion for the development of solid-state Li-air batteries.



Minghui Li received her Bachelor's degree in 2021 from Xiangtan University, and is now a graduate student in Zhengzhou University. Her current research interest focuses on solid-state Li–O₂ batteries.



Zhen Zhou received his BSc (applied chemistry, in 1994) and PhD (inorganic chemistry, in 1999) from Nankai University, China. He joined the faculty at Nankai University as a lecturer in 1999. Two years later, he began to work as a postdoctoral fellow in Nagoya University, Japan. In 2005, he returned to Nankai University as an associate professor and was promoted as a full professor in 2010. In 2021, he moved to Zhengzhou University, China as a Distinguished Professor, and he is now Dean of the School of Chemical Engineering. His main research interest lies in the integration of high-throughput computations, experiments and machine learning for energy storage and conversion.



Kecheng Pan received his Ph.D. degree in Tianjin University under the guidance of Prof. Suojiang Zhang, and is a research assistant in Zhengzhou University. His research interest includes solid electrolyte design and interface regulation of solid-state batteries.



Zhang Zhang received his Ph.D. degree in 2016 in Nankai University. Since 2021, he has been working at Zhengzhou University. His current research interest focuses on metal-air batteries.

2. Applicable Solid-State Electrolytes for Lithium-O₂ Batteries

2.1. Development of solid-state electrolytes

Between 1831 and 1834, Faraday laid the foundation for the study of solid-state ions by discovering the SSEs of silver sulfide and lead fluoride.^[15] Since Sony's first successful commercialization of LIBs in 1991, solid-state LIBs have also experienced rapid development.^[16] However, solid polymer electrolytes (SPEs) were not applied to LOBs until 1996 when Abraham and Jiang reported a non-aqueous thin film battery with polyacrylonitrile (PAN) polymers as Li⁺ conductors.^[17] They pressed the electrode and electrolyte layer together to form a 200 to 300 μm thick cell that exhibited an open-circuit voltage of about 3 V and a load voltage of 2.8 V, marking a significant milestone in the development of solid-state LIBs. Despite the development of SPEs, they typically utilized organic solvents like ethylene carbonate and propylene carbonate, which are susceptible to nucleophilic attacks of O₂⁻, resulting in irreversible decomposition. In 2012, Kitaura and Zhou made significant breakthrough in the development of SSLOB by using a Li anode, the Li_{1+x}Al_yGe_{2-y}(PO₄)₃ (LAGP) inorganic solid electrolyte (ISE), and a carbon nanotube (CNT) air electrode to construct a Li-air battery.^[18] However, Paoletta et al. discovered that LAGP could react with Li metal to form amorphous Li–Ge alloys after cycling, especially at higher temperatures, resulting in increased interface impedance and battery failure.^[19] They concluded that Ge was significantly reduced from Ge⁴⁺ to Ge²⁺ and Ge⁰. To address the interface contact issue between SPEs and ISEs, Zhu et al. developed a composite solid electrolyte (CSE) composed of polypropylene carbonate (PPC) and polyvinylidene fluoride-hexafluoropropene (PVDF-HFP) for the SPE and Li_{1.3}Al_{0.3}Ti_{1.7}(PO₄)₃ (LATP) for the ISE to improve mechanical properties.^[20] However, because LATP is as unstable as LAGP, and the polarization of the Li-air battery increases throughout the cycle, suggesting that more side reactions occur.

In recent years, substantial advancements have been made in the basic scientific research and industrialization of solid-state LIBs.^[21] However, due to the superior theoretical energy density, researchers have also begun exploring the potential of SSEs in LOBs. However, the reactions in LOBs not only include the process of Li⁺ shuttle between the cathode and anode, as in common Li batteries, but also involve the process of lithium reacting with oxygen at the cathode to generate solid discharge products. Also, it is important to consider the chemical stability of the electrolyte towards oxygen, as well as the three-phase interface involving the diffusion of oxygen and the availability of space for the storage of discharge products. Furthermore, the reversibility of the discharge products is another crucial factor that must be taken into account. The reaction and ion transport mechanisms are not yet fully comprehended for SSEs in LOBs,^[22] and further research is required to determine suitable SSEs for LOBs.

2.2. Categories of solid-state electrolytes

SSEs can be primarily categorized into three types: SPEs, ISEs, and CSEs.^[23] SPEs possess excellent flexibility, strong processability, low interface impedance, and a smooth and homogeneous interface with electrodes. However, they face challenges such as inadequate stability, low ionic conductivity at room temperature, and a narrow electrochemical window, which restrict their upper performance limits. ISEs, on the other hand, exhibit high ionic conductivity and mechanical strength but suffer from low overall conductivity and poor electrolyte-electrode contact. CSEs, however, provide a synergistic combination of the excellent performance of SPEs and ISEs. The structure and preparation process of CSEs can be further optimized.

2.2.1. Solid polymer electrolytes

SPEs typically form from the polymer matrices used as a solid solvent to dissolve lithium salts. Two main ion transport mechanisms have been found: one is structural rearrangement, namely diffusion between ion coordination sites through a jumping mechanism,^[24] and the other is fragment movement of coordination sites on the polymer backbone.^[25] Regardless of the transport mechanism, ion transport occurs mainly in the amorphous region rather than the crystalline region.^[26] Polyethylene oxide (PEO), as a solvent-free polymer electrolyte, was investigated on the O₂ electrochemistry in a solid-state cell by Hassoun et al.^[27] The oxidation of peroxides proceeds rapidly to singlet oxygen or more slowly to triplet oxygen, which depends on the lifetime of O₂^{*} in PEO and on the number of active collisions. Currently, researchers have also tested diverse polymer matrices, including polypropylene oxide,^[28] polyvinylidene fluoride (PVDF)^[29] and its copolymers with PVDF-HFP,^[7] polyvinyl alcohol,^[30] polymethyl methacrylate (PMMA),^[31] and PAN.^[17]

Since organic solvent decomposition affects battery performance, Balaish et al. first designed a liquid-free LOB based on SPEs in 2015, where the electrolyte was P(EO)₂₀LiTf (P(EO) = poly(ethylene oxide) and LiTf = lithium triflate).^[32] Generally, LOBs exhibit a capacity far below their theoretical limit due to sudden death and limited charge transport through the growing Li₂O₂ film to the Li₂O₂-electrolyte interface.^[33] However, researchers speculate that minor electrolyte decomposition in the polymer battery or O₂ diffusion could be a limiting factor in the battery's efficiency (Figure 2a). Although the battery exhibits poor electrochemical performance, the broad distribution of Li₂O₂ throughout the cathode and higher discharge voltage has demonstrated that PEO can serve as an electrolyte in LOBs. Then, due to the widespread use of PEO, its stability in LOBs has also been evaluated. As a recognized candidate polymer for SPEs, PEO has the advantages of high dielectric constant, good chemical structure and low glass transition temperature,^[34] which is conducive to promoting lithium salt dissociation and forming a binding Li–O₂ coordination with high chain movement. However, Balaish et al. strived to

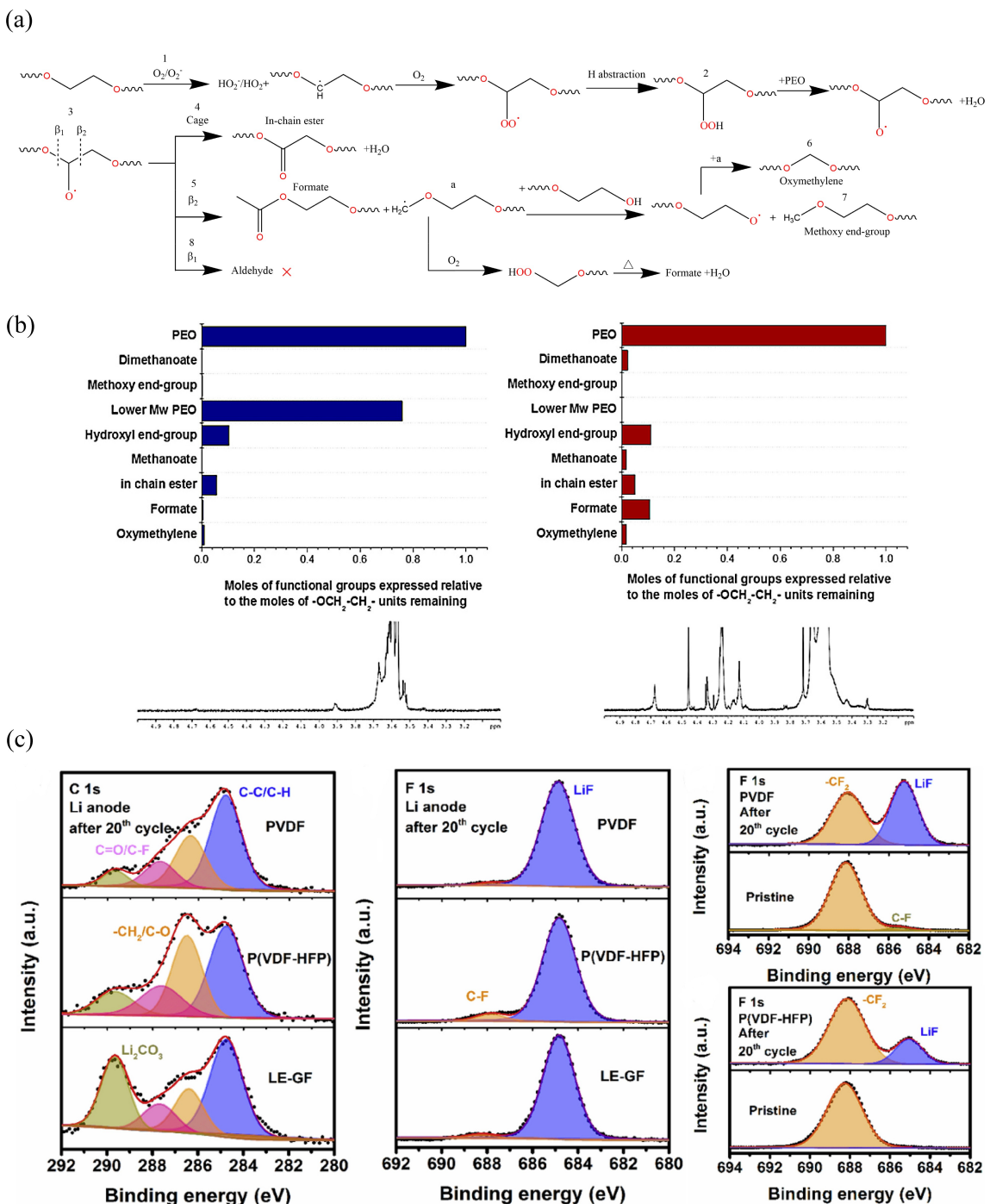


Figure 2. a) Proposed mechanism for degraded $\text{P}(\text{EO})_{20}\text{LiTf}$ electrolyte after discharged in a LOB at 0.05 mA cm^{-2} . Reprinted from Ref. [32] with permission. Copyright (2015) WILEY-VCH. b) Moles of various SPE degradation products relative to moles of $-\text{OCH}_2\text{-CH}_2-$ remaining units. Results were derived from quantitative ^1H NMR (Nuclear Magnetic Resonance Spectroscopy) spectra analysis after (left) discharge and (right) multiple discharge/charge cycles of SPE-LOB operated at 80°C under 1 atm O_2 . Reprinted from Ref. [35] with permission. Copyright (2018) American Chemical Society. c) XPS (X-ray photoelectron spectroscopy) of the Li anodes and the UDPE membranes in the symmetric Li–Li cells after the 20th cycle in O_2 atmosphere at a current rate of 0.2 mA cm^{-2} . C1s and F1s spectra of the Li anodes and F1s spectra of the UDPE membranes. Reprinted from Ref. [36] with permission. Copyright (2020) Elsevier.

advance the understanding of PEO degradation in the presence of the major discharge product, Li_2O_2 , after cycling at 80°C .^[35] Their findings revealed that the irreversible deposition of formate species and lithium formate-polymeric species resulting from the degradation of SPEs and the reaction between Li^+ and Li_2O_2 led to poor cycle performance (Figure 2b). Additionally,

the battery's low stability during extended operation at potentials higher than the open-circuit voltage would persist even if the PEO chain was minimized. Therefore, their results suggest that PEO-based polymers may not be a suitable choice for SPEs used in LOBs.

Yu et al. created ultra-dry polymer electrolytes (UDPEs) in 2020 without the use of any extra liquid.^[36] The cycle life of the UDPE-based catalyst-free LOBs under a high current density of 0.4 mA cm^{-2} is over twofold that of the LEs, which mainly arises from the formation of a stable LiF-containing solid electrolyte interface between UDPEs and Li metals (Figure 2c). However, the electrochemical performance of different lithium salts dissolved in PVDF-HFP matrix is limited by different aspects, namely electrochemical stability, ionic conductivity, interface stability, cycle stability or Li^+ transference number. Celik et al. reported in 2021 that different kinds and concentrations of dissolved lithium salts in PVDF-HFP copolymers have an impact on the electrochemical performance of LOBs.^[37] LiPF₆ salts endow SPE systems with the highest ionic conductivity, while LiTFSI (lithium bis(trifluoromethanesulphonyl)imide) has the widest electrochemical window and the highest Li^+ migration number. They found that 1.5 M LiTFSI: PVDF-HFP SPE has a high potential in LOBs, with an electrochemical potential window of 4.9 V and Li^+ migration number of 0.77.

Note that LOBs based on SPEs are currently limited by a range of factors, including chemical stability and mechanical strength.^[38] Furthermore, the low ionic conductivity of SPEs at room temperature is insufficient to meet the demands for LOBs. Consequently, researchers have explored several novel SPEs, including gel-polymer electrolytes (GPEs), dual-phase polymer electrolytes, single-ion-conducting polymer electrolytes, high-salt polymer systems, and nanocomposite conductors. GPEs, also known as quasi-solid polymer electrolytes (QSPEs), are generally considered an effective approach to addressing the aforementioned issues. These electrolytes consist of polymer networks that swell in solvents containing active ions. GPEs can be regarded as intermediate solution between typical LEs and "dry" SPEs.^[39] Apart from that, the liquid component of gels is immobilized in a polymer matrix and the membrane as a whole is virtually "solid" in character.^[40] Consequently, GPEs exhibit solid properties such as excellent mechanical properties, dimensional stability, and processability while still retaining the high ionic conductivity of LEs. GPEs and SPEs have different ion conduction mechanisms: SPEs conduct ions by interacting with substituents in the polymer chain, while GPEs mainly conduct ions in solvents or plasticizers.^[41] However, the presence of liquid components (or plasticizers) in gels can make them more susceptible to various redox reactions on the electrodes, ultimately leading to a decline in the battery's performance.^[42]

Liu et al. designed a sandwich-structured QSPE, which consists of PPC/Li-Nafion/PMMA.^[43] PMMA is used as the gelatinous cathode electrolyte and PPC as the solid anode electrolyte (Figure 3a). It is the first time to introduce Li^+ crosslinked polymers (Li-Nafion) into LOBs. The successful operation of the battery for 50 cycles (Figure 3b) demonstrates that the solution mechanism of Li_2O_2 still occurs with a 90% reduction in solvents. However, the sandwich structure and the stacking of three layers of materials, as well as the interfacial compatibility, result in low ionic conductivity of the electrolyte. Cho et al. conducted a study on a QSPE that utilizes polyethylene glycol methyl ether methacrylate as an ionic conductive agent and SiO₂ as a filler.^[44] The battery achieved

125 cycles at room temperature, and the QSPE exhibited significant electrochemical stability, as well as a high ionic conductivity of $1.4 \times 10^{-4} \text{ S cm}^{-1}$.

Zou et al. developed a GPE with a liquid component of tetraethylene glycol dimethyl ether (TEGDME) and nonwoven fabrics supported by the hydrogen bond between thermoplastic polyurethane and aerogel SiO₂.^[45] Although the morphology of SiO₂ used in the two investigations are different, both increase the ionic conductivity of the electrolytes and react with fresh dendrites to partially etch them away.^[46] The battery exhibits ultra-stable cycling performance at room temperature, and excellent durability of more than 20 days even under actual ambient air operating conditions (with a relative humidity (RH) of 40%). PVDF-HFP has become a more rational matrix for GPEs due to its advantages in mechanical properties, chemical corrosion resistance, and high temperature resistance. Zhao et al. developed a hybrid gel polymer electrolyte (HGPE) based on PVDF-HFP, in which MnOOH@Al₂O₃ as a porous nanowire membrane not only enhances the mechanical structure of GPEs and inhibits the growth of lithium dendrites, but also ensures the continuity of Li^+ conduction (Figure 3c), providing high Li^+ conductivity.^[47] LOBs with HGPE also have an ultra-long cycle life up to 494 cycles (Figure 3d). There are two ways to improve the conductivity of electrolytes: inhibiting the crystallization of polymer chains and increasing ion carrier concentration. Copolymerization,^[48] cross-link and the addition of inorganic materials can effectively reduce the crystallinity of polymers and increase the proportion of amorphous region, thus increasing the concentration of carrier ions in the system. Yang et al. designed a GPE consisting of PVDF-HFP/PMMA/SiO₂ in 2019 (Figure 3e).^[49] The electrolyte exhibits an organic-inorganic complexation structure in which two kinds of polymer cross-link, increasing the amorphous region in the electrolyte and enhancing the movement of the polymer chains, leading to the increase of Li^+ migration amount up to 0.62. LOBs assembled with this electrolyte can be operated for more than 300 cycles at room temperature. Besides, a dual polymer gel electrolyte (DGPE) networking strategy is proposed by Ren et al.^[50] In this design, trimethylolpropane ethoxylate triacrylate was used for in situ ultraviolet polymerization inside PVDF-HFP. DGPE is further combined with MnO₂/laser-induced graphene (LIG) cathode catalysts, prepared by direct laser writing on the polymer. Benefited from the inherent high activity of LIG and the stability of DGPE, the LOB cycles for 200 times at a cut-off capacity of 0.4 mAh/cm^2 and 50 times at a high current density of 0.4 mA/cm^2 with a high cut-off capacity of 2.0 mAh/cm^2 (Figure 3f). In addition to increasing ion concentration by changing solvent concentration, the strong polymer-solvent affinity would also enhance electrolyte uptake and Li^+ mobility. Liu et al. designed a PMMA and SiO₂ composite GPE (PMMA/SiO₂/PP@GPE), with which the LOB provides a high first charge and discharge capacity of 6.8 mAh cm^{-2} and stable cyclic performance of 116 times at 0.5 mAh cm^{-2} .^[31] The GPE has a high LE absorption capacity and sufficient gelatinization, which greatly improves electrochemical performance and interface stability.

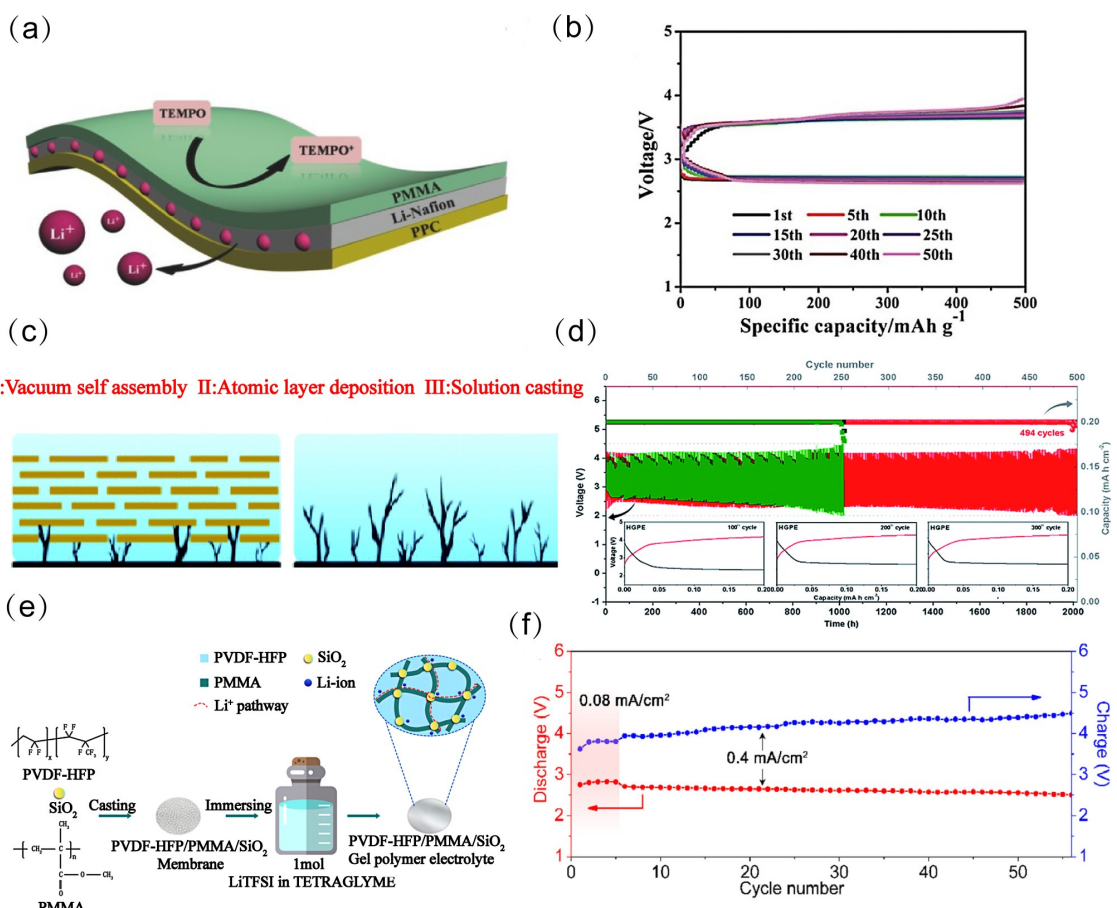


Figure 3. a) Schematic diagram of the PPC/Li-Nafion/PMMA membrane. b) Cycling performance of the QSPE cell at a current density of 100 mA g^{-1} . Reprinted from Ref. [43] with permission. Copyright (2017) WILEY-VCH. c) Schematic comparison of the Li dendrite growth in the HGPE and GPE. d) Electrochemical performance of LOBs with the HGPE and GPE at a current density of 0.1 mA cm^{-2} with a limited capacity of 0.2 mAh cm^{-2} . Reprinted from Ref. [47] with permission. Copyright (2019) The Royal Society of Chemistry. e) Composite diagram of SPE. Reprinted from Ref. [49] with permission. Copyright (2019) American Chemical Society. f) Discharge and charge mid-voltage vs. cycle number at a current density of 0.4 mA/cm^2 with limited capacity of 2 mAh/cm^2 . Reprinted from Ref. [50] with permission. Copyright (2020) American Chemical Society.

Although SPEs and GPEs have good mechanical flexibility, the growth of lithium dendrites still inhibits their practical applications. In addition, security problems caused by the use of a little organic LEs in GPEs continue to exist. Furthermore, the stability of SPEs and GPEs can be even worse for LOBs, as some polymers are not chemically stable towards Li and may even react with the discharge product. Therefore, achieving high ionic conductivity, mechanical strength, and stability simultaneously remains a challenge for SPEs and GPEs.

2.2.2. Inorganic solid electrolytes

ISEs are desirable owing to their safety, thermal stability and high ionic conductivity. The reported ISEs mainly included sulfide-type, perovskite-type, anti-perovskite-type, NASICON-type and garnet-type materials.^[51] Besides, the ion-conduction mechanisms in ISEs are significantly different from those in LEs. Solid-state ion conductors consist of mobile ions as well as metal and nonmetal ions that typically form polyhedral with ligands which create the skeleton of the crystal structure. Li⁺

conduction often depends on the defects in the crystal structure.^[52] To date, there have been several seminal reviews specifically devoted to the field of mechanism of ionic transport in solids.^[53] However, ISEs also suffer from two main problems. Firstly, due to their stiff and thick properties, there may be insufficient contact at the electrolyte/electrode interface.^[54] Secondly, there may be interfacial compatibility issues with either the anode or the cathode.^[55]

Due to the chemical instability of sulfide-type ISEs towards air,^[56] they were not used in Li-air batteries until recently in 2023. It was found that the main discharge product is Li₂O with a four-electron redox reaction pathway, rather than Li₂O₂ or LiO₂ (Figure 4a, b). In this work, the CSE of Li₁₀GeP₂S₁₂ and modified-PEO was adopted and the battery was able to cycle for 1000 times at room temperature (Figure 4c–e).^[57] Even though the discharge mechanism has been elucidated, it is nebulous whether the formation path of Li₂O due to electrons and Li cations (Reaction I, Figure 4f, step C) or Li₂O₂ disproportionation (Reaction II, Figure 4f, step F). The existence of nonstoichiometric Li_xO_y is uncertain, and it remains unclear whether it can be used as a new resource to generate Li₂O. As a

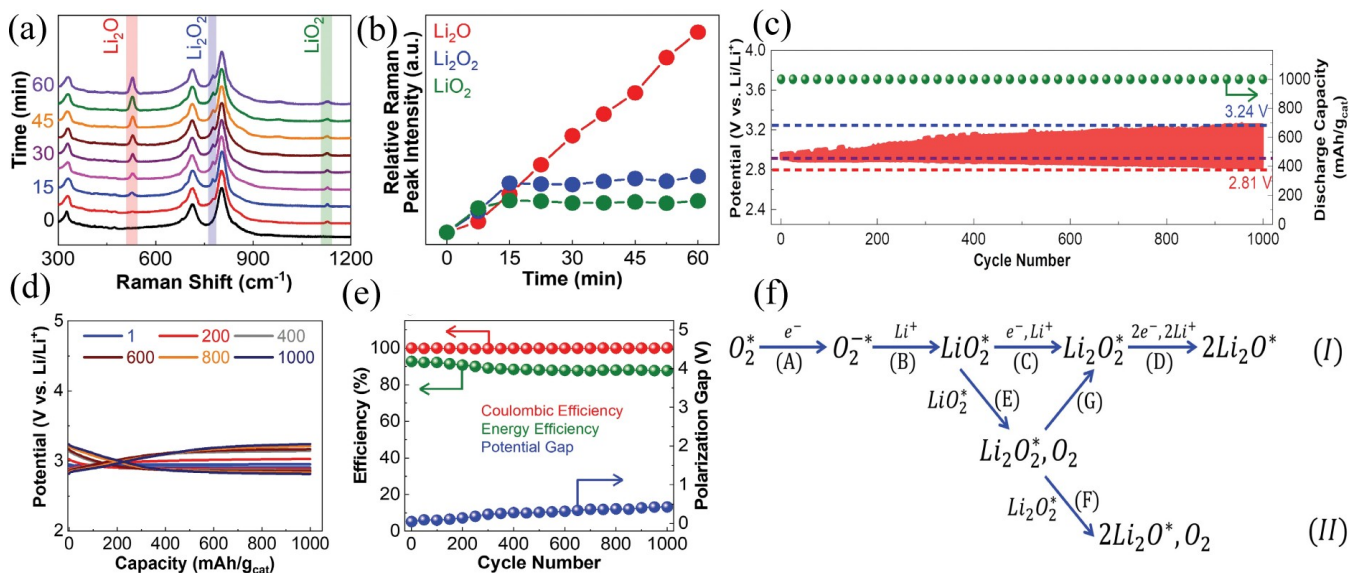


Figure 4. a) In situ Raman spectroscopy at different time intervals (capacity of ~125 mAh/g) during the discharge process at a current density of 1 A/g, indicating the evolution of peaks relevant to LiO_2 , Li_2O_2 , and Li_2O . b) Relative Raman peak intensities as the function of time during the discharge process. c) Galvanostatic cycling over 1000 cycles. d) Discharge/charge profiles at different cycles. e) Coulombic efficiency (red dots), energy efficiency (green dots), and polarization gap at the cycle end (blue dots) over 1000 cycles. f) Li_2O formation pathways. Shown are two reaction pathways to the formation of Li_2O based on the reaction of O_2 , Li^+ , and e^- . Reprinted from Ref. [57] with permission. Copyright (2023) Science.

result, the use of sulfide-type electrolytes provides an opportunity to build batteries with high energy density.

Lithium lanthanum titanate (LLTO), a typical perovskite-type solid electrolyte, has an electrochemical window larger than 4 V. However, it has limited ionic conductivity due to highly resistive grain boundaries.^[58] Le et al. present an original SSLOB composed of a porous structured Al-doped LLTO (A-LLTO) solid electrolyte with an integrated carbon layer and CoO nanoparticles as cathode catalysts for electrochemical reactions (Figure 5a).^[59] The LOB was highly stable up to 100°C and exhibited a long cycle life up to 132 times in the limited capacity of 500 mAh g⁻¹ at 0.3 mA cm⁻².

NASICON-type oxides are the most promising ISEs for Li-air batteries because of their high conductivity at room temperature,^[60] stability towards moisture and air, relatively low sintering temperature, and easy large-scale preparation. Among Li superionic conductors, LAGP and LATP are of importance for the development of SSLOBs. Kitaura et al. first reported an all-solid-state Li-air battery with LAGP, which showed reversible charge-discharge cycle performance in ambient air.^[18] The electrochemical reaction was found to occur around 3.1 V (vs. Li/Li⁺), which is similar to the redox potential of Li_2O_2 . In addition, some results indicated that the discharge product reacts with some gases such as H_2O and CO_2 in air, and side reactions occur. The operation of all-solid-state Li-air batteries need to be further improved. Some reports have presented that additives could further improve ionic conductivity by segregating along the grain boundary and facilitating the rearrangement of grains.^[61] B_2O_3 -added-LAGP (B-LAGP) glass ceramics show a room-temperature ionic conductivity of 6.7×10^{-4} S cm⁻¹.^[62] Although the ionic conductivity increases, the problem that LAGP reacts with Li still remains unsolved. A

compact, thin, and amorphous lithium phosphorous oxynitride (LiPON) layer could act as a protective interlayer for B-LAGP by separating it from the Li anode and mitigating the reaction between them. Jadhav et al. prepared LiPON/B-LAGP solid electrolytes through LiPON thin films depositing on B-LAGP by radio frequency-sputtering technique.^[63] While Zhang et al.^[64] and Wang et al.^[65] used LATP to circumvent the decomposition problem of LEs primarily. The Li^+ conductivity of the LATP sheet at 30°C is 3.8×10^{-4} S cm⁻¹. However, the great challenge in NASICON-type solid electrolytes is that Ge^{4+} and Ti^{4+} could be reduced when directly contacting Li metal. Therefore, when using such electrolytes, it is also necessary to consider how to protect Li anodes, which will be discussed in detail later.

Garnet-type oxides are the only kind of materials known to exhibit both high conductivity and compatibility with Li metal, making them highly promising for use in LOBs. Zhang et al. prepared a porous structure on the surface of $\text{Li}_{6.4}\text{La}_3\text{Zr}_{1.4}\text{Ta}_{0.6}\text{O}_{12}$ (LLZTO) by acid etching with an ionic conductivity of 1.2×10^{-3} S cm⁻¹, then infiltrated a trace amount of LEs containing 2,2,6,6-tetramethylpiperidinyloxy (TEMPO) and constructed a LOB together with the Li-Sn alloy anode.^[66] Due to the better wetting capacity of Li-Sn alloys, the interface resistance between the anode and LLZTO is significantly reduced. Benefiting from the synergy of TEMPO and dense ISEs in the porous framework infiltrating structure, the LOB can be cycled for 50 times at a charging voltage below 3.8 V. However, the formation of an insulating Li_2CO_3 layer on the surface of garnet-type SSEs and the high resistance at the SSE/electrode interfaces present critical challenges that need to be addressed.^[67] Thus, designing an ideal garnet-based LOBs requires comprehensive strategies for both eliminating the

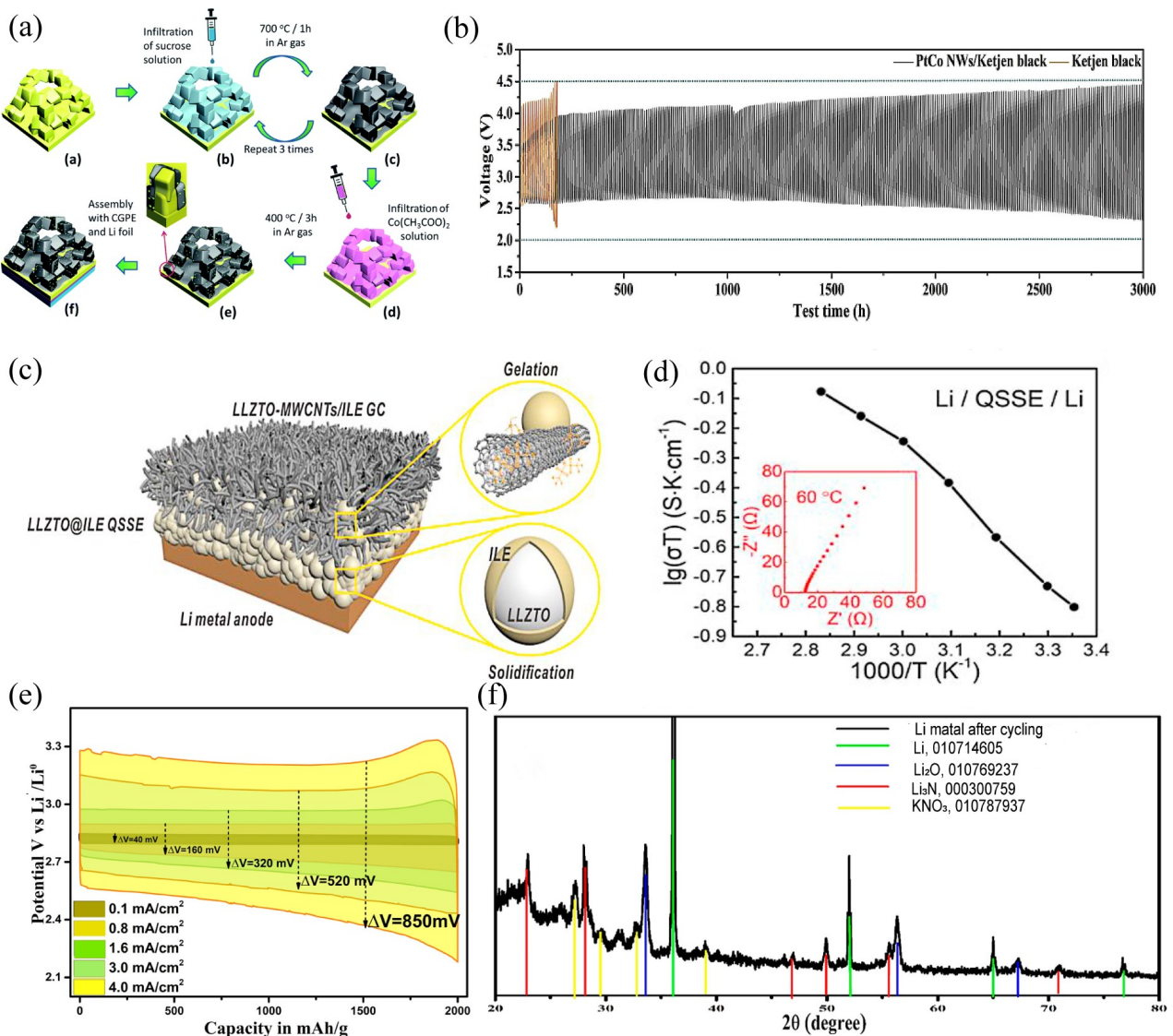


Figure 5. a) Schematic outlining the steps for the fabrication of a solid-state LOB composed of a Li metal anode, GPE interlayer, and solid electrolyte-integrated cathode where the porous A-LLTO solid electrolyte frame is covered with a carbon nanolayer and CoO nanocatalyst particles. Reprinted from Ref. [59] with permission. Copyright (2019) The Royal Society of Chemistry. b) Cycling performance of the quasi-solid LOBs with PtCo NWs/Ketjen black and Ketjen black as cathodes with a limited capacity of 500 mAh g⁻¹ at the current density of 100 mA g⁻¹ at 30 °C. Reprinted from Ref. [68] with permission. Copyright (2019) Elsevier. c) Schematic representation of the LOB based on MWCNTs-LLZTO/ILE gel cathode and LLZTO@ILE QSE. d) Arrhenius plot and EIS of QSE at 60 °C. Reprinted from Ref. [69] with permission. Copyright (2020) Elsevier. e) Rate performance of LOB in LiNO₃:KNO₃:CsNO₃ (37:39:24) electrolyte at 140 °C at current density ranges from 0.1 to 4.0 mA/cm² in voltage window 2–3.4 V. Cathode: VC + PVDF (90:10). Anode: Li metal. O₂ pressure: 1 bar. f) Anode after cycling in molten LiNO₃:KNO₃:CsNO₃ (37:39:24) electrolyte LOB. Reprinted from Ref. [71] with permission. Copyright (2018) American Chemical Society.

Li₂CO₃ layer and reducing the resistance at the SSE/electrode interfaces.

In addition to GPEs, ionic liquids can also form an inorganic ion gel matrix with an inorganic matrix, providing advantages such as improved thermal stability and mechanical performance. At present, SiO₂ with simple preparation and adjustable diameter of size and pore, has been the most common inorganic matrix. Xing et al. integrated the synergistic effect of highly active Pt₃Co nanowires (PtCo NWs) cathode catalysts and a stable quasi-solid SiO₂-ionic liquid electrolyte (ILE).^[68] PtCo NWs can effectively reduce the charging voltage lower than 3.2 V, while the SiO₂-ILE has a high ionic conductivity. The LOB can be reversibly discharged and charged for more than

300 cycles (>3000 hours) (Figure 5b) and the lithium anode is subject to its perfect protection of SiO₂-ILE. Additionally, Gao et al. prepared LLZTO@ILE combined with multi-walled carbon nanotubes (MWCNTs) to prepare a gel cathode (Figure 5c).^[69] The solidified ILE shell and space charge region in the yolk-shell LLZTO@ILE structure improved the transport of Li⁺, and the electrolyte exhibited high ionic conductivity up to 1.71×10^{-3} S cm⁻¹ at 60 °C (Figure 5d). The cations in ILE and the π electrons in MWCNTs form a 3D continuous electrochemical interface of electrons, ions and oxygen to provide high battery performance.

Although ISEs typically offer higher conductivity for faster charging, all-solid-state LOBs manufactured with current tech-

nologies fall short of achieving their theoretically attainable high volumetric energy density. Xiao et al. reported a subversive manufacturing technology,^[70] which imitates the low-cost manufacturing process of commercial LEs in LIBs. They used SSEs with a low melting point that infiltrated the dense and thermally stable electrode in a liquid state at a moderately elevated temperature (around 300°C or lower) and subsequently solidified during cooling, significantly reducing the obstacles to industrial application. Similarly, Karkera et al. investigated LiNO₃-KNO₂-CsNO₃ (37:39:24) eutectic salt mixture at 140°C as a molten electrolyte for LOBs, which exhibited low charge-discharge overpotentials of 40 mV and cycle up to 200 times (Figure 5e).^[71] The significant reduction in overpotential is attributed to the faster charge transfer kinetics of molten electrolytes and better solubility of discharge products. Molten nitrate LOBs involve slightly different reaction mechanisms compared with the conventional non-aqueous batteries. LiNO₃ based molten electrolytes create an in-situ protection layer containing Li₂O and Li₃N on Li metal anodes to sustain stable LOBs at lowest ever overpotentials (Figure 5f). Finding a porous, anticorrosive cathode compatible to molten nitrate environment and heat inputs to liquefy the eutectic mixture, would permit to realize a practical LOB.

2.2.3. Composite solid electrolytes

In the current SSEs, multiphase CSEs have greater flexibility and customize the advantages of single-phase electrolytes. Although ISEs can inhibit the growth of Li dendrites, they also tend to exhibit high interfacial resistance to electrodes. SPEs offer additional advantages in scalability and processability to facilitate large-scale preparation. However, SPEs have relatively low ionic conductivity and require operation above room temperature. Introducing inorganic fillers into SPEs to improve the ionic conductivity of CSEs, and nanoparticle-type fillers could form a continuous network to avoid particle agglomeration.^[72] Generally speaking, the current research on CSEs used in LOBs can be divided into three categories: inorganic-organic CSEs, organic-organic CSEs and inorganic-inorganic CSEs. The inorganic-organic CSE, which was further divided into "ceramic-in-polymer", "intermediate" and "polymer-in-ceramic" according to the proportion of ingredients, is the most widely investigated and will become the focus of this review.

Typically, Yi et al. took advantage of amorphous LiNbO₃ with low grain boundary resistance and high Li⁺ diffusivity combining with poly(methyl methacrylate-styrene) (PMS) to construct a CSE for LOBs.^[73] Stemming from the contribution of amorphous LiNbO₃ to the copolymer chain movement, the ionic conductivity of the electrolyte is higher than that of pure PMS. To further enhance the interface stability, the researchers developed lithium-salt-modified single-walled CNTs and ionic liquid-based crosslinking network gels (CNGs), and provide efficient channels for electrons, ions, and oxygen. Meanwhile, the temperature significantly influences the electrochemical behavior of the LOB.^[74] In particular, Yi et al. designed a CSE

with LAGP and PMS to unravel the electrochemical behavior of CSE-based LOBs at high temperature.^[75] A unique CNG composed of lithium salt modified single-walled CNTs and ionic liquid is used as the cathode. By introducing ionic liquids to the cathode at high temperatures, Li⁺ migration restrictions triggered by drying of ether-based solvents can be avoided, resulting in improved cycling performance (350 cycles) (Figure 6a, b). Note that the carbon-based cathode used in this work was unstable at high temperatures in the presence of highly reactive oxygenated substances, such as O₂⁻ and O₂²⁻. Avoiding side reactions associated with carbon materials at high temperatures by using carbon-free cathodes presents significant opportunities for enhancing the cycle life of future solid-state Li-air batteries operating at high temperatures.

The affinity between the amorphous SiO₂ and the polyethylene glycol dimethyl ether solvent leads to the formation of a cured gel electrolyte and increased salt dissociation. In similar cases, Gu et al. designed a double-layer organic-inorganic CSE.^[76] On account of its compatibility with Li anodes, poly(ethylene-glycol) methyl ether methacrylate is as a polymer buffer layer. Besides, Si doping can promote the movement of Li⁺ in the LAGP lattice, exhibiting a higher ionic conductivity of 3.7×10^{-4} S cm⁻¹. Thanks to the synergistic effect of poly(ethylene-glycol) methyl ether methacrylate and Si-LAGP, the initial charge and discharge capacity of the LOB reaches 7.3 mAh cm⁻².

Despite its high ionic conductivity (over 10^{-4} S cm⁻¹) and excellent chemical stability, the development of LAGP as a candidate for LOBs is hindered by the possibility of Ge⁴⁺ reduction in SSE.^[77] In view of this, Wang et al. developed a CSE with a rigid Li_{1.5}Al_{0.5}Ge_{1.5}(PO₄)₃ core@ultrathin flexible PVDF-HFP shell interface.^[78] The ultrathin flexible PVDF-HFP shell provides soft and stable contact between the rigid core and Li metal, inhibiting Ge⁴⁺ reduction caused by direct contact with Li metal. LAGP not only acts as a structural enhancer to achieve high Young's modulus but also constructs Li⁺ diffusion network to homogenize Li⁺ distribution (Figure 6c). The LOBs offer long stability of 146 cycles (Figure 6d), which is more than three times that of GPE-based LOBs. Except NASICON-type ISEs, the rest can also be used to prepare CSEs. For example, Le et al. made a composite GPE in 2016 by using PVDF-HFP polymer and Al-doped Li_{0.33}La_{0.56}TiO₃ particles covered with a modified SiO₂ layer, and the battery could operate for 1922 h.^[79]

Another perovskite-type ISE, LLZO, Song et al. used it and PEO to construct a three-dimensional LLZO-PEO solid electrolyte, in which LLZO can inhibit polymer crystallization and promote the segmented movement of polymer chains.^[80] The three-dimensional LLZO structure eliminates particle agglomeration and provides a continuous and efficient polymer/filler interface. The ionic conductivity of the electrolyte is 9.2×10^{-5} S cm⁻¹. However, the oxidative degradation of PEO as an electrolyte is also problematic. A typically known polymer like PMMA shows excellent electrochemical stability (including the stability to Li metal and to O₂⁻ during charge and discharge). Wang et al. used organic PMMA and inorganic modified MgO to make a stable hybrid SSE.^[81] Since oxygen-containing functional groups could shorten path of original ion

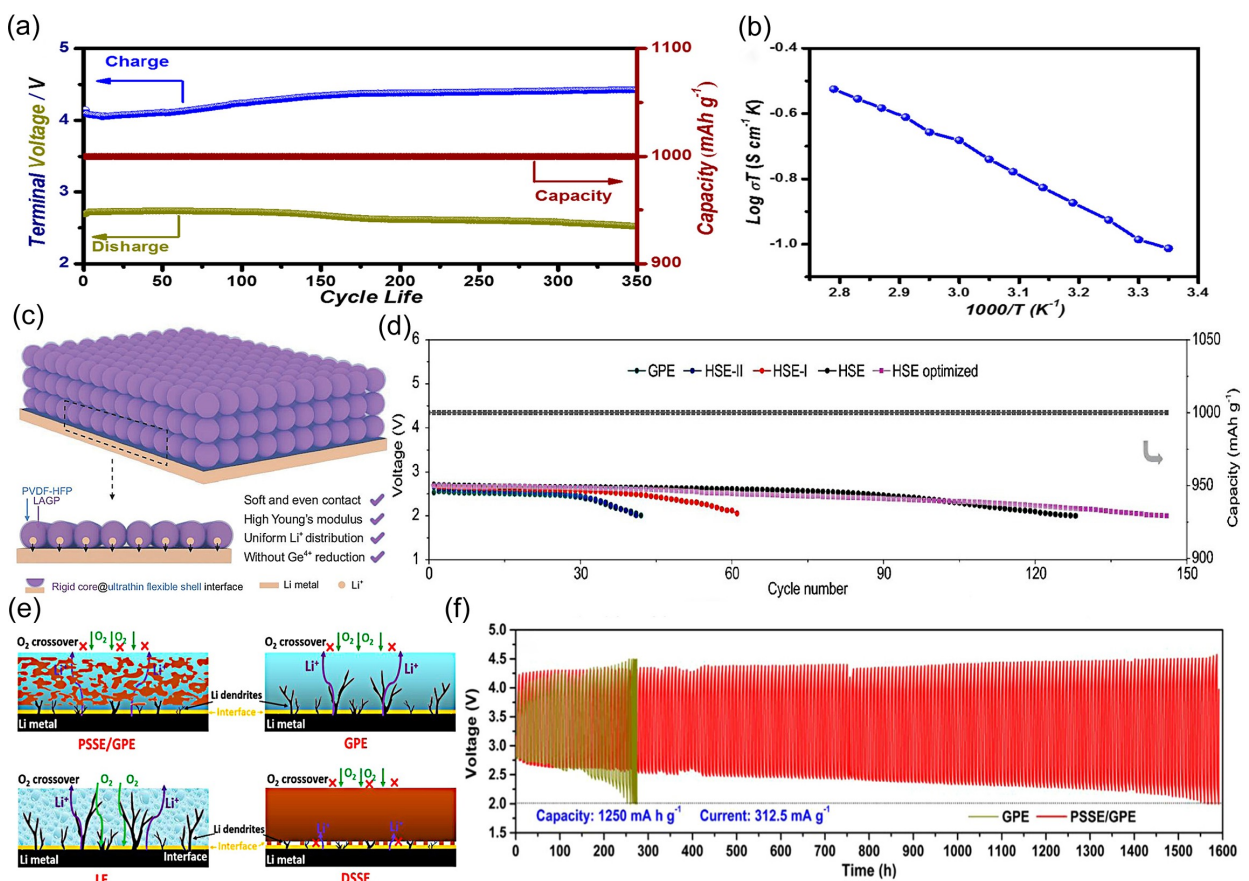


Figure 6. a) Terminal voltage with cycle life of SSLOBs under dry O_2 at 50 °C. b) Arrhenius plots of Li ionic conductivities of the HSE at elevated temperature. Reprinted from Ref. [75] with permission. Copyright (2017) American Chemical Society. c) Schematic representation of dendrite-free lithium deposition enabled by HSE. d) The cycle life of QSE LOBs with different electrolytes. Reprinted from Ref. [78] with permission. Copyright (2021) Science. e) Schematic comparison of the effects of various electrolytes in LOBs. f) The corresponding discharge/charge profiles during the cycling performance test. Reprinted from Ref. [82] with permission. Copyright (2020) American Chemical Society.

conduction, the battery has a good ionic conductivity and a wide electrochemical window. Although PMMA and MgO are combined, their joint effect is not clearly explained and the stability of PMMA to O_2^- needs to be further explained.

In addition to the influence of the composition of SSEs, the combination mode between inorganic and organic electrolytes will also have a great impact on the battery performance. Zhao et al. proposed a CSE with PMMA and LLZTO, which consists of three-dimensional porous garnet microstructures and GPE.^[82] In addition, the CSE can block O_2 penetration (Figure 6e), and the battery has a long cycle life of 194 times and a high cycle capacity of 1250 mAh g⁻¹ (Figure 6f). Besides, Wang et al. designed a unique hybrid electrolyte system with an organic/ceramic/organic electrolyte architecture, where the ceramic electrolyte is LLZT containing Al₂O₃.^[83] The addition of Al₂O₃ fills the ceramic gap and increases the density. Since Li₂CO₃ tends to appear at grain boundaries and holes, the addition of Al₂O₃ will reduce the formation rate of Li₂CO₃. Due to the introduction of garnet electrolytes, the potential difference to which organic electrolytes are subjected is reduced. Thus, the decomposition of organic electrolytes is suppressed, and thereby protects the Li anode. This provides a new way for more research concerning a novel electrolyte system for LOBs.

There are also some other ways to combine CSEs. For instance, Jung et al. combined a GPE of PVDF-HFP and ionic liquid to construct a CSE in LOBs.^[84] The ionic liquid of PYR₁₄ (N-methyl-N-butyl-pyrrolidinium) has a wide potential window, which can improve the stability of Li metal in the long-term cycle. The crystalline phases of PVDF were converted from type II of non-polar conformation into type I of zig-zag conformation and intermediate polar conformation, which was due to the addition of LiTFSI and PYR₁₄TFSI induced polymer chain rearrangement. Therefore, the ionic conductivity values of the ionic liquid-GPE were determined to be 3.6×10^{-4} S cm⁻¹ at 30 °C higher than those of the (PVDF-HFP)-LiTFSI composite. Also, ionic liquid-GPE leads to the formation of a more conductive and stable solid electrolyte interface (SEI) on Li metal, and provides a more effective barrier for the transmission of water to Li anodes. Besides, Man et al. prepared a poly(ethylene glycol) diacrylate (PEGDA)-SN-LiTFSI thermal crosslinked polymer electrolyte, since the polymer molecular chain, the content of succinonitrile (SN) and crosslinking time all affect conductivity.^[85] The electrochemical stability window reaches 5.2 V and the conductivity is 1.76×10^{-4} S cm⁻¹.

CSEs indeed offer several advantages over other types of solid electrolytes. By combining different compositions, CSEs

can harness the beneficial properties of each component, such as the high ionic conductivity and mechanical stability of inorganic electrolytes and the flexibility of polymer electrolytes. This allows for improved overall performance, including enhanced ion transport, electrochemical stability, and reduced interfacial resistance compared with single-component solid electrolytes. Additionally, CSEs can exhibit higher flexibility and processability, and provide more choice and possibility for the design and manufacture of batteries. Furthermore, the oxygen resistance of the composites can resist the attack of strong oxidative intermediates and products, and the porosity can provide space for discharge products. Overall, CSEs have shown promise in addressing the challenges associated with solid-state batteries and have the potential to enable high-performance and safer LOBs.

3. Challenges and Strategies

The high energy density of SSLOBs has garnered significant attention in recent years, but their development is currently hampered by several challenges. To improve the application of SSEs in LOBs, adjustments must be made to the anode and cathode to meet the necessary requirements. Firstly, the anode/cathode should be chemically stable for the electrolytes and not undergo any chemical reactions. Secondly, the interface between the electrode and electrolyte should have fine compatibility to minimize interfacial resistances. Furthermore, to construct an ideal SSLOB, it is essential to design an anode that is superior in handling Li dendrites and volume change, and a cathode that has high electronic conductivity, fast mass transfer, and oxygen diffusion. Therefore, optimizing the anode/cathode and regulating the interface is crucial.

3.1. Anode optimization

Li metal with extremely low redox potential (-3.04 V vs. SHE) and ultra-high theoretical capacity (3862 mAh g^{-1}) is an ideal anode for batteries.^[86] Nevertheless, Li metal itself has huge problems, and the serious safety risk restricts its further development. Firstly, Li metal has very high chemical and electrochemical reactivity, which will result in corrosion and low utilization rate. Secondly, during the continuous Li plating process, an uneven Li^+ flux distribution near the electrode surface will cause the uneven Li deposition due to the existence of local space charge layer, thus producing dendrites. Finally, Li anodes suffer from huge volume expansion and contraction during long-term Li plating/stripping processes, leading to lower coulombic efficiency and shorter cycle life. In this regard, it is critically necessary to develop novel strategies to improve the stability of Li anodes. To tackle these challenges, significant effort has been devoted to developing new strategies such as coating a physical/chemical protective layer on the surface of Li anodes, modifying the SEI and implementing experimental techniques.

To overcome the drawbacks of nonaqueous LOBs, a hybrid electrolyte was developed by combining aqueous and organic electrolytes with a water-stable LAGP. However, safety concerns arise when the brittle ceramic plate fails to effectively separate the organic and aqueous solutions. To enhance the chemical stability of the interface between the anode and SSE, Bao et al. developed a lithium biphenyl (LiBP) liquid anode to replace Li metal, and deposited a Ti layer on the anode of the ceramic plate (Figure 7a–c).^[87] LiBP is less reactive than Li in contact with aqueous solutions, which results in a more stable battery system. Also, adding alloying elements such as Si, Al, and Sn can improve the stability of Li metal. Zhang et al. used a Li–Sn alloy to promote a tighter contact between the anode and LLZTO electrolyte.^[66] Due to the better wetting capacity of Li–Sn alloys, the interface resistance between the anode and LLZTO is significantly reduced. Although the stability of alloy anodes is relatively high, its capacity is lower than that of Li metal.^[88] Therefore, enhancing the stability of Li metal remains a primary research focus. Wu et al. built a superhydrophobic H_2O -preventing QSE to develop a LOB with Li anodes in a humid atmosphere (RH is 45%) (Figure 7d).^[89] The SSE is composed of super hydrophobic SiO_2 matrix and Li^+ -conductive IL, with strong heat resistance (no obvious decomposition below 230°C), high electrochemical stability (>5.5 V), and high ionic conductivity ($9.1 \times 10^{-4}\text{ S cm}^{-1}$) and super hydrophobicity (contact angle $>150^\circ$). More importantly, they facilitate to suppress H_2O cross over from the cathode to Li anode.

3.2. Cathode optimization

The cathode plays a crucial role in the electrochemical reaction in a LOB by providing the reaction sites for three phases: Li^+ , O_2 , and the catalyst.^[90] Firstly, the carbonaceous materials are instable in the presence of Li–O species with high reactivity, forming irreversible Li_2CO_3 and other side products at the interface.^[91] Secondly, the by-products of LOBs, such as carbonates and carboxylates, are difficult to decompose even under high voltage, affecting battery efficiency and cycle life. Finally, the growth of Li_2O_2 particles within the solid-state cathode (SSC) is limited (<50 nm in thickness) because of the poor electron/ion transport in Li_2O_2 .^[92] For further advancement of SSLOBs, demonstration of rationally optimized design for cathodes is an important step. Additionally, SSEs are not in full contact with cathodes compared with LEs. Due to the absence of a liquid medium for Li_2O_2 growth, the capacity is limited in SSLOBs. Specially, the specific capacity and cyclic stability of LOBs are largely overestimated.^[93] Hence, the choice of a stable cathode material with effective functions must therefore be designed to greatly increase reversibility.

Several studies have proposed to replace carbonaceous materials due to their instability in the presence of Li_2O_2 .^[94] Pakseresht et al. designed one-dimensional MnO_2 polymorphism (α -, δ -, γ - MnO_2) by biological template method and the surface of α - MnO_2 nanowires combined with Ru nanoparticles is an effective carbon-free cathode material.^[95] The use of an integrated GPE/cathode structure could greatly improve the

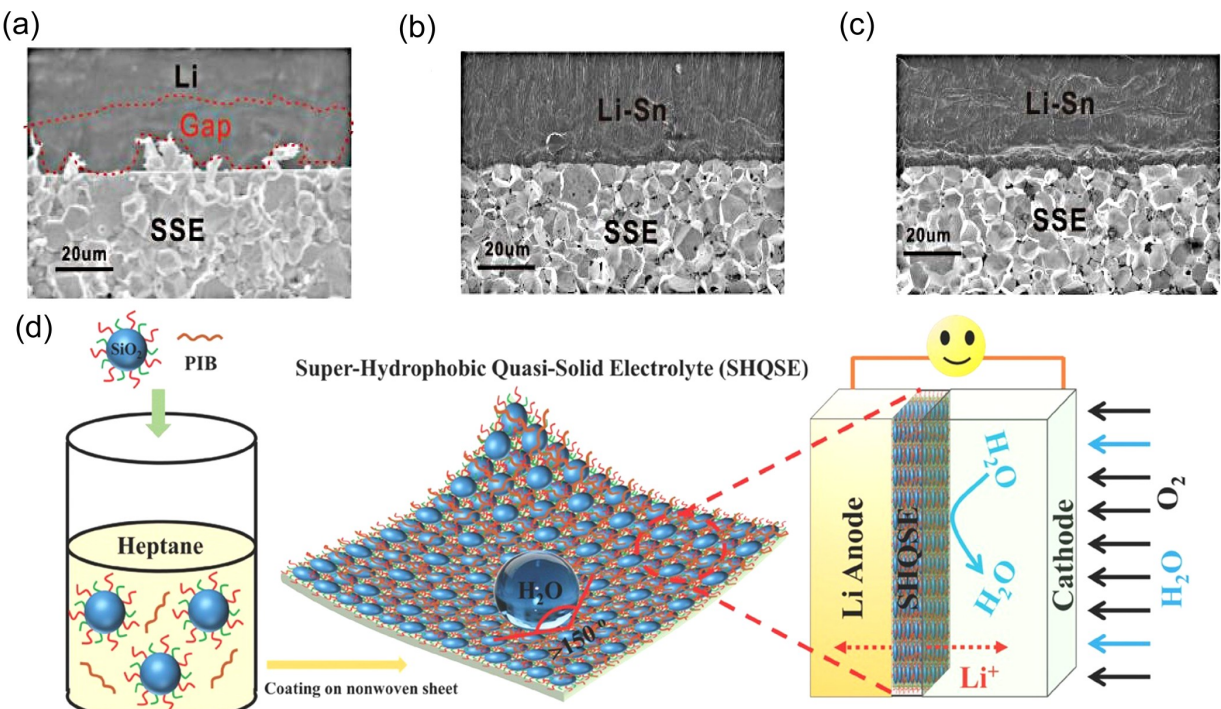


Figure 7. a) SEM (scanning electron microscope) images for cross-section of pure Li/SSE interface. b, c) SEM images for cross-section of Li-Sn/SSE interface before and after 200 h cycles at 0.4 mA cm^{-2} . All electrochemical tests were conducted at 30°C . Reprinted from Ref. [66] with permission. Copyright (2020) The Royal Society of Chemistry. d) Schematic of the proposed solid LOBs in humid atmosphere based on the superhydrophobic H₂O-preventing QSE. Reprinted from Ref. [89] with permission. Copyright (2016) Wiley-VCH.

stability and cycling performance of the LOB. In addition, Kim et al. designed the highly conductive ruthenium-based composite (RBC) as a carbon-free cathode (Figure 8a).^[96] They simultaneously added water vapor as an additive to alter the discharge products from Li₂O₂, which has limited growth, to LiOH. Additionally, the use of RBC as both an electronic and ionic conductor was able to eliminate the parasitic chemistry of conducting carbons, resulting in over 665 cycles of successful operation (Figure 8b). However, in comparison with the small amount of water, the charging voltage is excessively high in the presence of air, probably due to the generation of Li₂CO₃. As a result, additional measures are necessary to mitigate the impact of CO₂ in the future, in order to develop a more practical and reversible battery in the air. Some reports have introduced an oxygen selective membrane that only allows oxygen to enter the battery. Zhu et al. designed a new type of Li-air battery with a silicon oil film coated hole to block H₂O and CO₂ in the air (Figure 8c).^[97] The new Li-air battery without silicon oil films outputs $23728 \text{ mAh g}_{\text{carbon}}^{-1}$ without reversibility. In contrast, the battery with silicone oil films can output a discharge capacity of $11697 \text{ mAh g}_{\text{carbon}}^{-1}$ and can be fully charged (Figure 8d). The existence of silicone oil films can avoid the generation of side reactions and make the reaction process reversible in air.

The development of the cathode in SSLOBs has been hindered by low practical capacity, as the reported capacity did not take into account the weight of the electrolyte in most papers, which is significantly higher than the cathode.^[98] Thus,

improving the capacity is a critical issue that needs to be addressed for the practical application of LOBs. Wang et al. fabricated an inorganic solid-state air cathode (10 wt% Super P carbon, 85 wt% LATP powder, and 5 wt% PVDF).^[65] Although the porous air cathode provided a sufficient O₂-transport channel facilitating a high discharge capacity, the decomposition of carbon seriously deteriorated the cycling performance. Therefore, introducing more stable cathode materials is key to achieving practical application. Besides, the stability of other materials (the binder, current collector, and so on) also requires meticulous care. Then, they studied the influence of water vapor (key component in the air) on the LOB with solid-state air cathodes.^[99] Interestingly, the amount of Li₂CO₃ generated in the presence of wet O₂ was lower than that in dry O₂. This may be attributed to the formation of LiOH, which obstructed the direct interaction between the carbon and Li₂O₂.

3.3. Interface between the electrolyte and anode

Due to loss of liquid wettability and unstable interface between Li anodes and electrolytes, there is huge uneven current distribution at the solid-solid contact interface, because physical contact makes surface contact to point contact. In addition, Li metal can react with the majority of ISEs. The primary drawback of polymer films utilized in LOBs is their limited strength. However, incorporating ISEs with a polymer membrane can enhance its mechanical strength, flexibility, and hardness,

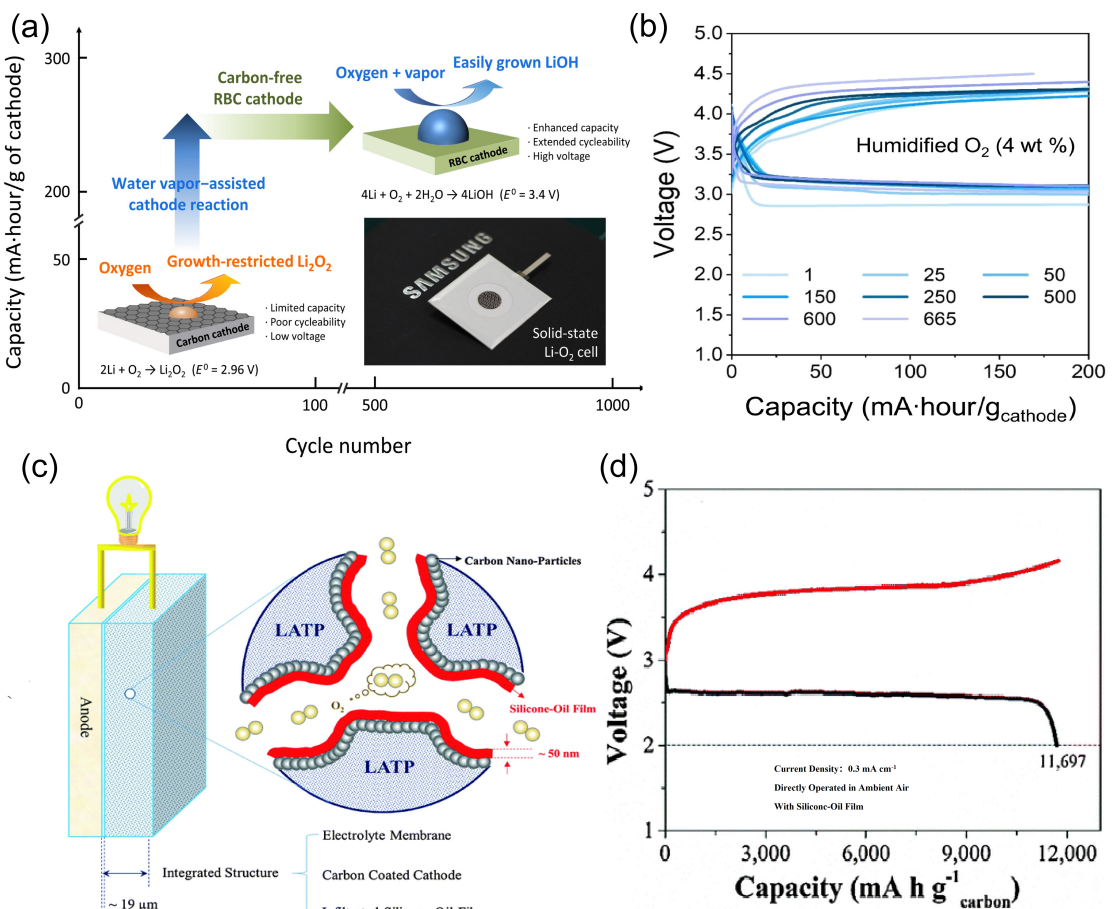


Figure 8. a) Schematic illustration of proposed SSLOBs. Discharge behavior of SSLOBs with RBC cathodes during operation in dry and humidified O_2 atmosphere with added water vapor. b) Long-term discharge-charge profiles of cells with 200 mAh/g_{cathode} for representative cycle numbers. Reprinted from Ref. [96] with permission. Copyright (2022) Science. c) The proposed solid-state Li-air batteries with an integrated structure of the solid-state LATP membrane, carbon-coated LATP cathode and a silicone-oil film inside the cathode. d) Typical galvanostatic charge/discharge curves of the proposed Li-air batteries with a silicone-oil film operated in ambient air (~50% RH) at a constant current density of 0.3 mA cm⁻². Reprinted from Ref. [97] with permission. Copyright (2015) The Royal Society of Chemistry.

effectively impeding the growth of Li dendrites and safeguarding the Li anode. In the same way, heterogeneous deposition and dissolution of Li cause growth of lithium dendrites, which can penetrate the diaphragm, further leading to a short circuit and decreased battery capacity.^[100] Thus, the key to improving battery performance lies in maintaining the stability of the Li anode throughout the cycling process.^[101]

There are several options of surface treatment available for interface modification of Li metal, including electrochemical pretreatment, chemical pretreatment, polishing pretreatment, and deposition of a protective film. These treatments can regulate the composition and structure of the SEI film.^[102] Regarding electrochemical pretreatment, Lim et al. reported to use PEO as a SEI layer coating on a Li anode under O_2 through an in-situ electrochemical pre-charging step.^[103] This approach generates stiff Li_2CO_3 and LiF components that are uniformly distributed throughout the anode, resulting in a mechanically and chemically robust surface film (Figure 9a). This evenly distributed SEI layer interacts with a flexible polymer matrix to form a submicrometer-sized gel-like polymer layer. This polymer-supported SEI layer results in a much longer cycle life as

compared with the original battery under the same test conditions (Figure 9b). Protective coatings deposited via atomic layer deposition or molecular layer deposition offer precise control over thickness and conformity, making them a relatively simple and scalable industrial application to protect Li metal. Sun et al. reported a nanoscale inorganic-organic functional “gradient coating” with a controlled gradient composition based on inorganic Zn composition by the molecular layer deposition (Figure 9c).^[104] The outer layer of the coating consists of an electrically insulating polymer polyurea to confine the electrodeposition of Li below the surface, while the lithophilic Zn site is introduced into the inner layer to promote uniform Li nucleation and further deposition. The LOB with this coating has stable cycling performance for 1500 hours (Figure 9d).

Strengthening the isolation effect of the separator can effectively suppress the corrosion of the Li anode and the interaction between the anode and cathode in LOBs. Besides, the uneven distribution of Li^+ flux on the surface of Li anodes is also considered an important cause of dendrite formation.^[105] Polyether-ketone has a more appropriate pore size, narrower pore size distribution, and higher porosity compared with glass

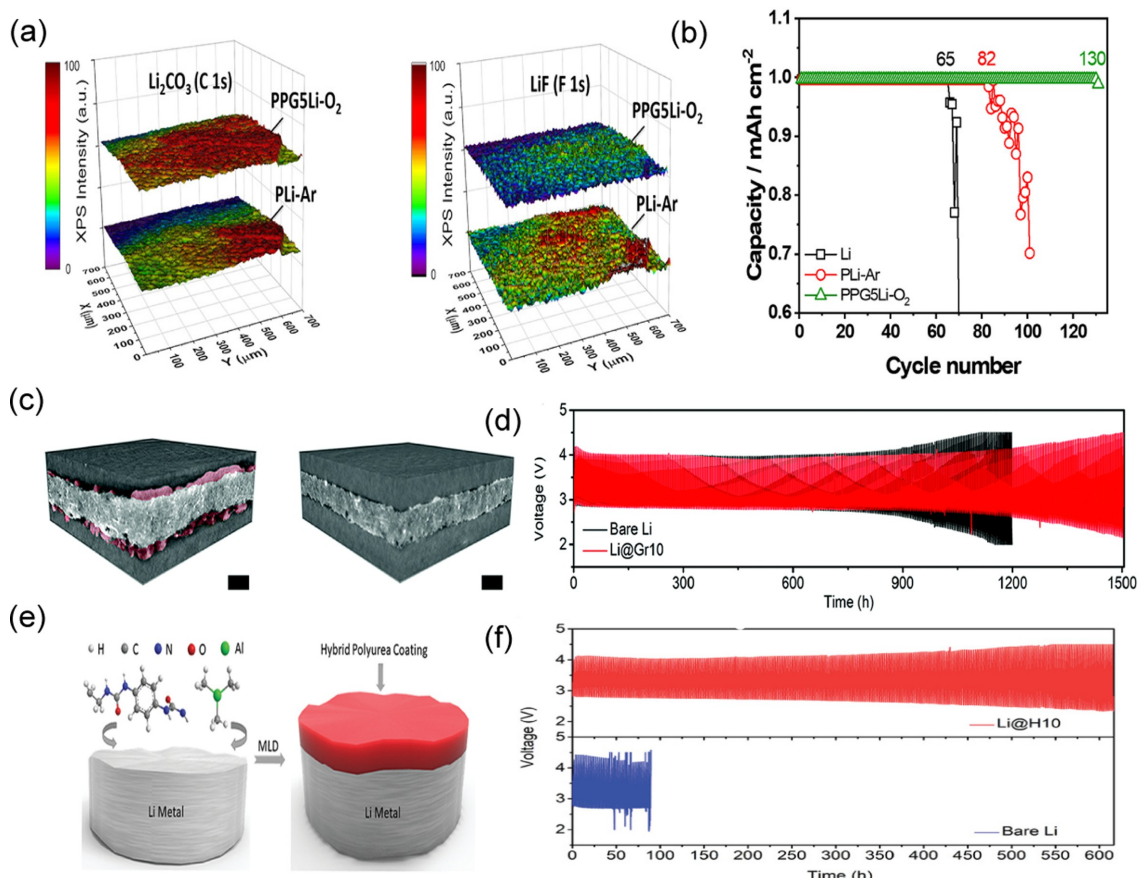


Figure 9. a) XPS images showing the distribution Li_2CO_3 and LiF compositions on the surface of Li metal anodes with and without PEO-based gel polymer coatings (5 wt% of PEO in PEO-based gel polymer) from the pretreated LOB at 0.2 mA cm^{-2} to 5 V of charge cutoff voltage under Ar or O_2 atmosphere, respectively. b) Cycle life at a current density of 0.2 mA cm^{-2} under a capacity limited protocol of 1.0 mAh cm^{-2} in the cutoff voltage range of 2–5 V. Reprinted from Ref. [103] with permission. Copyright (2021) American Chemical Society. c) 3D renderings for the symmetric cells after electrochemical cycling using (left) bare Li and (right) Li@Gr10 (10 cycles of gradient coating on Li, 'reacted Li' is highlighted by red color). The lengths of scale bars are $200 \mu\text{m}$. d) Discharge/charge profiles of LOBs using bare Li and Li@Gr10 for an areal capacity of 0.2 mAh cm^{-2} . Reprinted from Ref. [104] with permission. Copyright (2021) The Royal Society of Chemistry. e) Schematic showing the synthesis procedure of the molecular layer deposition hybrid polyurea coating for enhanced mechanical property. f) Electrochemical performance of LOB with Li@H10 (10 cycles of HPU on Li) and bare Li. Reprinted from Ref. [108] with permission. Copyright (2020) WILEY-VCH.

fibers and polypropylene. These factors affect the transport of Li^+ in the separator and ultimately allow polyether-ketone to inhibit the growth of lithium dendrites. Sun et al. developed a soluble precursor polymer by incorporating a "protective" group into the monomer.^[106] This precursor polymer was then converted into a nanofiber membrane through a simple acid treatment process, ultimately resulting in a polyether-ketone nanofiber membrane. The membrane prepared by this chemically induced crystallization method exhibited high cycle stability, which circulates 194 times under 200 mA g^{-1} with curtailing capacity of 500 mAh g^{-1} . However, these gel layers do not provide sufficient mechanical strength to suppress dendrite outgrowth. Hsia et al. fabricated a dense and completely dry PVDF-HFP layer, and coated it directly on the Li anode.^[107] Compared with fiber separators, PVDF-HFP has a lower diffusion rate and greater resistance of Li^+ . Besides, it reduces the diffusion rate difference between ions and inhibits the growth of lithium dendrites. In addition, its relatively non-porous characteristics can prevent moisture and O_2 in air from entering

the surface of Li metal, effectively reduce metal corrosion and promote the stable transmission of Li^+ .

Although the battery is more stable, its maximum peak power density is significantly lower than that of glass fiber separators, and the SSE interface mechanism is not clear. While polymer-based films are flexible, they normally have limited mechanical strength. Inspired by inorganic fillers for mechanical enhancement of polymers, Sun et al. reported a mixed inorganic-organic polyurea film as an artificial SEI for Li anodes, and trimethylaluminum was introduced into the polymer chain as a cross-linker (Figure 9e).^[108] The artificial SEI effectively inhibits dendrite formation and, thanks to its electrical insulation properties, can adjust the Li plating and stripping process. As a result, the LOB incorporating this film can operate for more than 600 hours (Figure 9f).

The SEI film on the surface of Li metal is formed as a result of the reaction between the metal and the electrolytes, including organic solvents and supporting electrolytes. Thus, by adjusting the organic solvent, supporting electrolyte, or incor-

porating additives, the composition of the SEI membrane can be optimized to improve the overall performance of the LOB. Regarding the organic solvent, Zhu et al. developed a QSE consisting of a PVDF-HFP/PPC polymer matrix, LATP inorganic ceramic electrolyte, LiTFSI salt, and a TEGDME/PMIMTFSI (1-propyl-3-methylimidazolium bis(trifluoromethylsulfonyl)imide)hybrid plasticizer.^[20] They discovered that the stable interface between the SSE and Li anode was mainly achieved by the formation of a protective layer containing fluoride and the $-CF_3$ group, which resulted from the in-situ decomposition of PMIMTFSI during the cycle. At a limited capacity of 1000 mAh g^{-1} , the LOB cycled 196 times at a current density of 400 mA g^{-1} . On the other hand, Liu et al. developed a stable and hydrophobic CSE comprising thermoplastic polyurethane and hydrophobic SiO_2 nanoparticles.^[109] They coated this CSE onto the Li anode to promote homogeneous Li^+ transfer and inhibit Li dendrite growth. Also, Zhao et al. prepared a LOB composed of PVDF-HFP polymer, TEGDME solvent and LiClO_4 salt.^[110] Thanks to the unique property of PVDF-HFP, the polar β -phase PVDF-HFP has a high dielectric constant and an intensive affinity with Li^+ . This composite has the ability to regulate and redistribute Li^+ , thereby inhibiting the formation of Li dendrites and reducing the accumulation of "dead Li". As a result, the battery incorporating this composite can operate stably for over 1100 hours and achieve 553 cycles.

Inserting a protective layer or constructing a suitable SEI on the Li anode via in situ reaction can improve the interface contact and Li^+ transport, thereby reducing side effects. Additionally, introducing a small number of film-forming additives during the in-situ SEI building process is favorable to further reduce interface resistance and effectively improve cycle stability. Finally, the in-situ forming technique provides a promising prospect for achieving physical contact between the electrolyte and electrode in SSLOB.

3.4. Interface between the electrolyte and cathode

Despite SSEs solve the major problems of organic electrolytes, SSLOBs are still in their infancy and lots of scientific and technological problems imposed by SSEs, like limited triple-phase boundaries (TPBs) in the SSC, large resistance, and poor stability of SSEs, need to be solved. TPB between the SSE and cathode is a key location affecting the transport of Li^+ , e^- and O_2 , serving as active sites, to facilitate the electrochemical reaction. In addition, the interfacial resistance also has a significant impact on the discharge capacity. However, there are two conflicting requirements which make the design of satisfactory SSCs really a challenging task. The diffusion of O_2 and sufficient space to accommodate the discharge products demand the SSCs to be porous, while the transfer of Li^+ and e^- requires SSCs to have continuous channels.^[111] Therefore, the development of a convenient and valid strategy to construct SSCs with abundant TPBs simultaneously is highly desired.

Most cathodes for SSLOB are prepared by simply mixing the SSE and carbon material, or directly sintering carbon on the SSE pellet to construct an integrated cathode-electrolyte structure

(ICES). Li et al. prepared the integrated structure of the ISE and cathode by using convenient one step sintering, which consists of a dense $\text{Li}_{1.5}\text{Al}_{0.5}\text{Ge}_{1.5}\text{P}_3\text{O}_{12}$ layer and a carbon coated polar LAGP layer.^[112] Although the battery showed a relatively high discharge capacity of 0.48 mAh cm^{-2} at $5 \mu\text{A cm}^{-2}$, it could sustain six full cycles with a restricted capacity of 0.08 mAh cm^{-2} at $10 \mu\text{A cm}^{-2}$. Thus, this approach is not suitable for SSLOBs, as it may not deliver good electrochemical performance due to the different substances used in LAGP and carbon, which can lead to increased interfacial resistance. Along with this integrated architecture approach, Zhu et al. sintered a 96% of the dense LATP electrolyte layer onto a 75% of the porous LATP cathode support, and prepared a multi-layer carbon nanostructure into a porous LATP scaffold.^[113] The bottom layer is composed of fine carbon nanoparticles, providing a large amount of TPBs for electrochemical reactions, and the top layer is composed of overlapping carbon nanofibers, providing a large space for the storage and O_2 transport of solid products (Figure 10a). The cathodic TPBs in this battery are found to be 330 times larger than those in conventional SSLOBs. This design enables the battery to withstand 1174 cycles (equivalent to 150 days) at 0.5 mA cm^{-2} (as shown in Figure 10b), with stable coulombic efficiency (100%) and an energy efficiency decrease of no more than 10% (from 72.6% to 65.1%). Furthermore, Le et al. fabricated the cathode frame and the SSE layer by using the same A-LLTO ceramics, which allowed for the formation of a seamless interface between the two components after sintering at high temperatures, resulting in negligible interface resistance.^[59] Moreover, taking into account the good compatibility between the electrolyte and electrode, which results in a relatively small interface resistance in GPE, Xiao et al. developed an integrated architecture of GPE-nanoarray cathode.^[114] In this design, the precursor solution for GPE was incorporated in advance into a self-standing, binder-free cathode consisting of Co_3O_4 nanosheet arrays grown on carbon cloth ($\text{Co}_3\text{O}_4@\text{CC}$), and the photo-initiated in situ polymerization of GPE was conducted on this integrated structure. The solid state GPE has abundant interface contacts with the electrode, which helps enhance charge transfer and mass diffusion, and provides sufficient active sites for the catalytic oxygen reduction and evolution reaction. Moreover, Song et al. developed a cathode supported QSE with an integrated composite polymer-based architecture (ICPA).^[115] The integrated structure is constructed by CSE with PEO, lithium salt and LLZO cast on the composite cathode. Compared with the common cathode, it shows lower charge transfer impedance. As the interface impedance between the electrolyte and the cathode decreases, the TPBs become more established. ICPA-based batteries achieve significantly high discharge capacity and low performance degradation. Although the CSE could improve the ionic conductivity and high mechanical properties, it cannot form a continuous network and avoid particle agglomeration. To this end, Li et al. designed a flexible ICES to achieve tight connections by supporting on a 3D SiO_2 nanofibers framework (Figure 10c).^[116] The 3D SiO_2 nanofibers act not only as a bridge connecting the CSE and the cathode, but also as 3D ceramic fillers and porous cathode carriers to increase the ionic conductivity of CSEs and

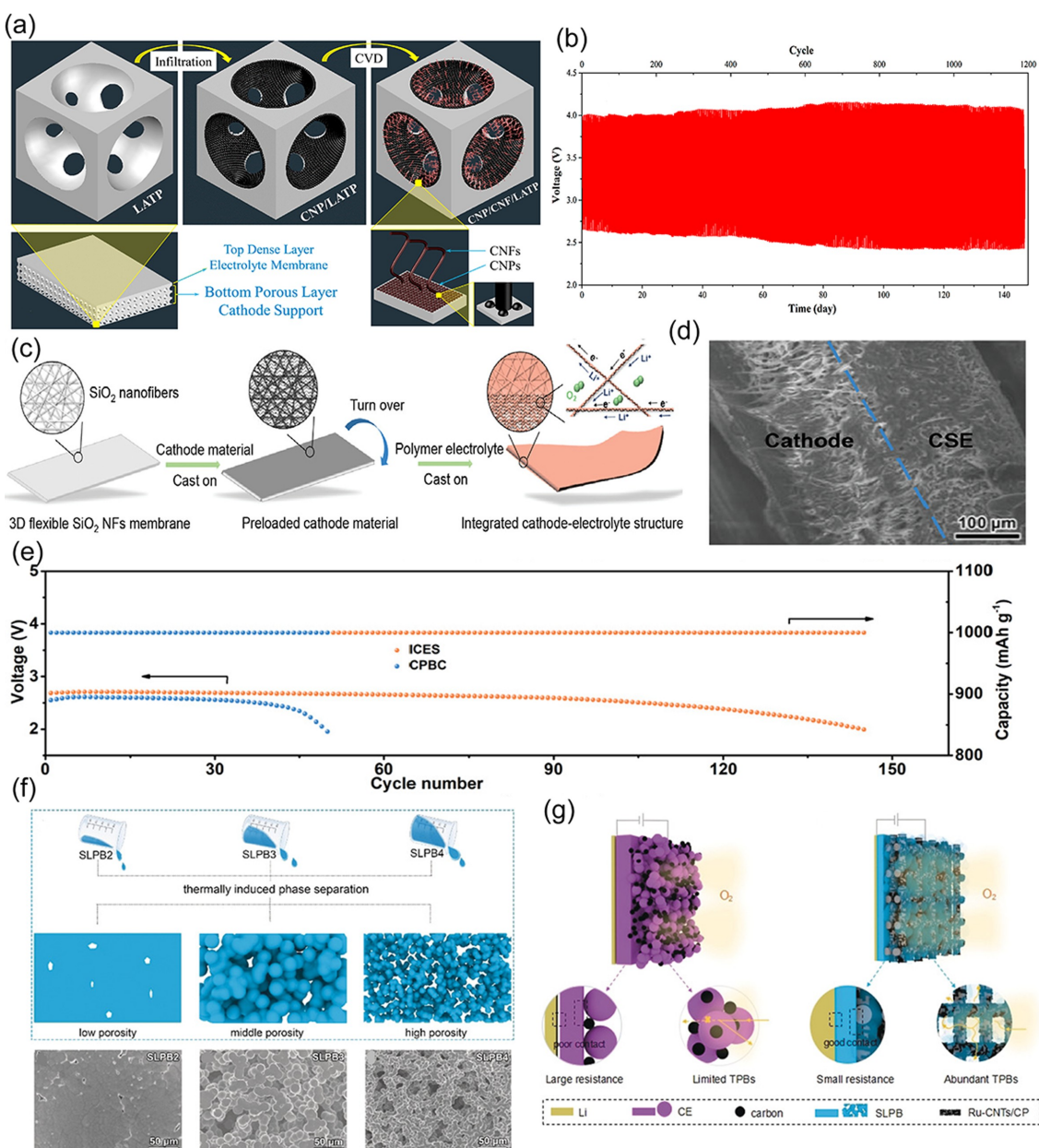


Figure 10. a) Schematic representation of architectures for a seamless electrolyte-electrode structure, which is prepared with glass-ceramic LATP, the top dense layer serves as electrolyte-membrane while the bottom porous layer serves as cathode-support. b) Discharge-charge profiles with cycling of the proposed Li-air battery with a CNPs (carbon nano-particles) and CNFs (carbon nano-fibers) successively coated LATP cathode in pure O_2 at 0.5 mA cm^{-2} under a capacity limitation of 0.75 mAh cm^{-2} . Reprinted from Ref. [113] with permission. Copyright (2016) Elsevier. c) Schematic of the preparation process of the ICES with 3D SiO_2 NFs membrane as a supporting framework. d) Cross-sectional SEM image of the ICES. e) Cycling performance of the SSLOBs at a limited capacity of 1000 mAh g^{-1} and a current density of 500 mA g^{-1} . Reprinted from Ref. [116] with permission. Copyright (2022) Wiley-VCH. f) Schematic illustration of the preparation of SLPB (SN-based PCE). SEM images of SLPB2, SLPB3, and SLPB4. g) Schematic illustration of (left) the conventional SSLOB with CE (ceramic electrolytes) and (right) the SSLOB with adjustable-porosity SLPB. Reprinted from Ref. [117] with permission. Copyright (2020) Wiley-VCH.

reaction sites in the cathode (Figure 10d). The battery has a high discharge capacity and a long life of 145 cycles, with a cycle capacity of 1000 mAh g^{-1} at 60°C (Figure 10e). Furthermore, taking inspiration from the simplicity and controllability of thermally induced phase separation, Wang et al. constructed SN-PCE (plastic crystal electrolytes) with adjustable porosity into the carbon cathode to construct SSCs with abundant and continuous TPBs (Figure 10f, g).^[117] This approach facilitated the transfer and rapid diffusion of Li^+ / e^- and O_2 within the battery system. At the same time, the flexibility and adhesion of SN-PCE

significantly reduce the resistance and the presence of a large number of pores increases the O_2 diffusion rate, which is conducive to the TPB reaction. However, the existence of nitrile group in SN-PCE will lead to instability of Li, that is, the side reaction of Li catalyzed nitrile polymerization will occur, similar to the polymerization of $\text{C}\equiv\text{N}$ in SN in $\text{Na}-\text{CO}_2$ batteries.^[118] In recent years, various modification methods have been developed in an attempt to prepare SN-based SSEs with high Li^+ stability.^[119]

Generally, multiple large interfacial resistance exists between the SSC and electrolyte, resulting in high discharge/charge polarization and rapid failure. Therefore, minimizing the number of interfaces and distributing the essential ionic/electronic contacts evenly are potential approaches. Zhao et al. used a mixed conductor of electrons and ions to build SSCs with nitrogen doped carbon nanotubes (NCNTs) and LiTaO₃.^[120] By turning the point-to-point interface into a face-to-face interface, they significantly improved the electrochemical active area of the cathode. Due to accessibility of Li⁺ on NCNT-LiTaO₃ cathodes, the effective electrochemical active area with fast ion and electron transfer leads to discharge specific capacity 7023 mAh g⁻¹ at a current density of 1000 mA g⁻¹.

Simply mixing the SSE and cathode material is unable to build an effective TPBs. However, a large number of micropores and a large specific surface area can effectively increase the TPB once the surface area of the cathode is fixed. The current mainstream methods involve extending TPBs from the traditional electrolyte/cathode interface to the entire cathode and constructing a whole porous structure by directly loading catalytic active components onto the three-dimensional ordered layered SSE. However, the key and challenging problem is to expose more active sites and regulate the translation of electrons or protons between different interfaces to solve the interface problem essentially.

3.5. Redox mediators in solid-state Li–O₂ batteries

Redox Mediators (RMs) for solution-induced decomposition of discharge products are receiving intense research interest in virtue of ameliorating sluggish kinetics and increasing energy efficiency.^[121] In the past a few years, many RMs have been developed, including the most commonly used inorganic Li compounds such as LiI,^[122] LiBr,^[123] LiCl,^[124] and LiNO₃,^[125] as well as organic redox-active species including tetrathiafulvalene (TTF),^[126] TEMPO,^[127] 5,10-dihydro-5,10-dimethylphenazine,^[128] and a group of quinone derivatives. RMs, different from solid-state catalysts, are soluble in LEs. Although it is difficult to use RMs with SSLOBs, researchers have tried to use RMs in LOBs based on GPEs.

Among all proposed RMs, LiI has been extensively studied in LOBs as it possesses a low oxidation potential vs. Li/Li⁺ of about 3.3 V.^[125] However, the "shuttle effect" of RMs causes new problems. Shi et al. prepared a GPE by using a sulfonation strategy with sulfonated bacterial cellulose (SBC) and employed LiI as the redox mediator.^[129] Benefiting from the high-density negatively charged SO_3^- groups on the SBC, GPEs can generate a strong electrostatic repulsion force on negatively charged I₃⁻ and inhibit the shuttle effect of LiI-RM (Figure 11a, b). TEMPO, which is sterically protected by four α -methyl groups, is a persistent radical that demonstrates high electrochemical stability and fast diffusion kinetic.^[127] Hou et al. prepared a QSE by using self-made Nafion membrane with controllable thickness, PVDF-HFP and TEMPO.^[130] As a single-ion conductor, the Nafion membrane within the polymer layer could selectively permeate Li⁺, and effectively block RMs. This

allowed the LOB to recycle up to 50 times. Sultana et al. introduced pBQ (1,4 benzoquinone) into the methyl silyl terminated polyether polymer electrolyte to significantly improve electrochemical performance with a low overpotential of 0.8 V (Figure 11c, d).^[131] At the same time, Li₂O₂ forms a film shape on the cathode surface. This outstanding achievement of LOBs based on polymers and RMs paved the way for a new method of commercialization of SSLOBs. Inspired by superoxide dismutase (SOD) in biological systems, Ren et al. assumed that SOD mimics can also be used in LOBs to catalyze the dismutation of O₂^{•-}.^[132] Due to the interaction between O₂^{•-} and oxidized activated charcoal (OAC), OAC was added to a dual GPE to change the basic mechanism of LOBs (Figure 11e, f). The redox cycle of OAC can fully reduce the soluble LiO₂, thereby reducing the side reaction caused by the soluble LiO₂.

3.6. Integrated design

After the above detailed discussion, it is evident that extensive efforts have recently been dedicated to enhancing the performance of cathodes, anodes, and electrolytes in LOBs. Successful integration of these components may prove an effective strategy for simultaneously addressing the major challenges associated with LOBs. Huang et al. reported on a graphene-based quasi-solid-state LOB.^[133] This battery comprises a well-designed three-dimensional porous graphene cathode, a GPE modified with RMs, and a porous graphene/Li anode (Figure 12a). First of all, the porous graphene cathode (Figure 12b) offers a high surface area and significant porosity, thereby providing a high-density of active sites for O₂ reduction and TTF oxidation, as well as ample channels to facilitate the transport of O₂, Li⁺, and TTF. Secondly, The GPE-TTF composite provides low Li⁺ diffusion resistance, mitigates the shuttle reaction between TTF and the graphene/Li anode, inhibits electrolyte volatilization, and reduces the formation of Li dendrites. In addition, TTF can mediate the oxidation of Li₂O₂ under low overpotential, alleviate the decomposition of GPE and inhibit side effects. Thirdly, the porous graphene/Li anode (Figure 12c) simultaneously solves the problems of dendrite growth and infinite volume change of Li anodes. Therefore, these three components are indispensable and crucial to ensure the excellent electrochemical performance of solid LOBs.

A novel integrated prototype battery was designed to integrate all components into one unity. Chi et al. developed an integrated solid-state Li-air battery that incorporates an ultra-thin, high-ion-conductive Li⁺-exchanged zeolite X (LiX) membrane as the sole SSE.^[134] This battery utilizes an in-situ assembly strategy to integrate cast Li as the anode and CNTs as the cathode (Figure 12d). Most notably, the LiX-based battery demonstrates a high capacity of 12020 mAh g⁻¹. Moreover, when operated at a current density of 500 mA g⁻¹ and a capacity cut-off of 1,000 mAh g⁻¹, the battery exhibits an impressive cycle life of 149 cycles (Figure 12f). This far exceeds the cycle life achieved by batteries with LAGP (12 cycles) and organic electrolytes (102 cycles) (Figure 12e). Furthermore, the large-scale production of SSLOBs at low cost and flexible SSEs

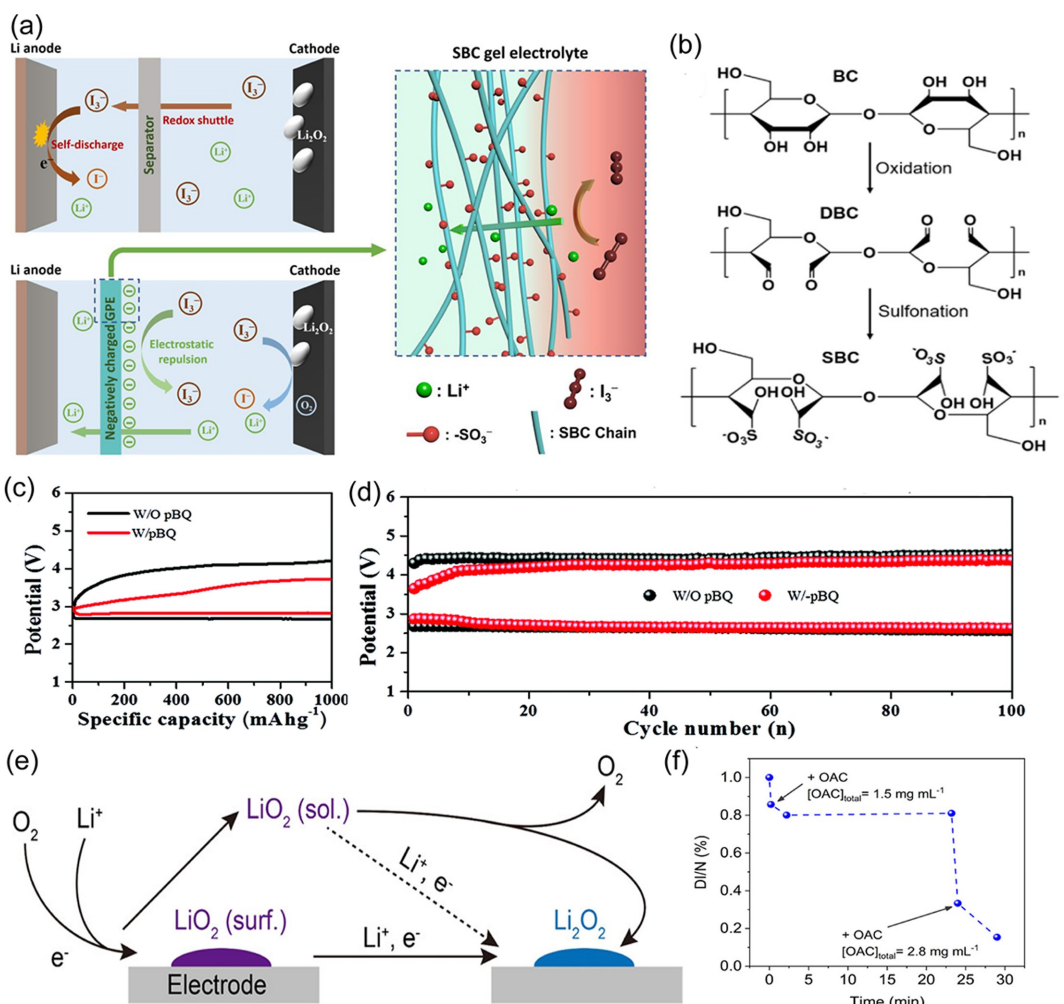


Figure 11. a) Schematic illustration of the functional GPE preventing I_3^- shuttling through electrostatic repulsion. b) Structural changes of BC during the oxidation and sulfonation process. Reprinted from Ref. [129] with permission. Copyright (2021) American Chemical Society. c) The comparisons of discharge and recharge potentials in LOBs using a polymer electrolyte w/and w/o pBQ at a current density of 200 mAh⁻¹. d) Comparison of charge-discharge potentials for the polymer electrolyte w/ and w/o pBQ in LOBs for 100 cycles. Reprinted from Ref. [131] with permission. Copyright (2021) The Royal Society of Chemistry. e) Discharge process of oxygen to LiOH in LOBs with dual GPE-OAC as the separator and electrolyte. f) Integrated EPR (electron paramagnetic resonance) signal intensity versus incubation time with OAC. Normalized double integration (DI/N): the area under the absorptive signals. Reprinted from Ref. [132] with permission. Copyright (2021) American Chemical Society.

would be feasible, which also provides a possibility for practical application of other solid energy storage systems.

The improvement of individual components is not satisfactory enough to achieve the best performance of full cells without bringing various other problems. Given that, by the synergy of all components, the device-level design may be the superior construction of batteries. Firstly, the most critical aspect is to identify appropriate materials for the electrolyte, cathode, and anode that exhibit adequate mechanical or chemical stability. Secondly, it is important to consider the synergistic effects of all components, as failure to do so may result in side reactions and decomposition issues. Finally, the mode of combination determines the stability of the overall battery, which further affects the specific capacity, cycle performance, rate capacity, as well as safety, stability, and flexibility.

4. Summary and Perspectives

In this review, we summarize recent progress of typical SSEs for LOBs, including SPEs, ISEs and CSEs (Table S1, Supporting Information). Moreover, we discuss the main challenges associated with SSE-based LOBs. Although great progress with irreplaceable security advantages has been achieved in current SSLOBs, extensive investigations are still desired to meet the requirements for practical applications. There are still many unsolved mysteries and considerable debates surrounding SSEs; therefore, multiple systematic and integrated research efforts are needed to create a powerful LOB firstly in the laboratory. To achieve this goal, not only a combination of research studies on SSEs is required, but also investigations into air cathodes, Li anodes, interface chemistry and cell configurations.

Firstly, the most pressing concern is to identify a suitable SSE that offers exceptional ionic conductivity while maintaining

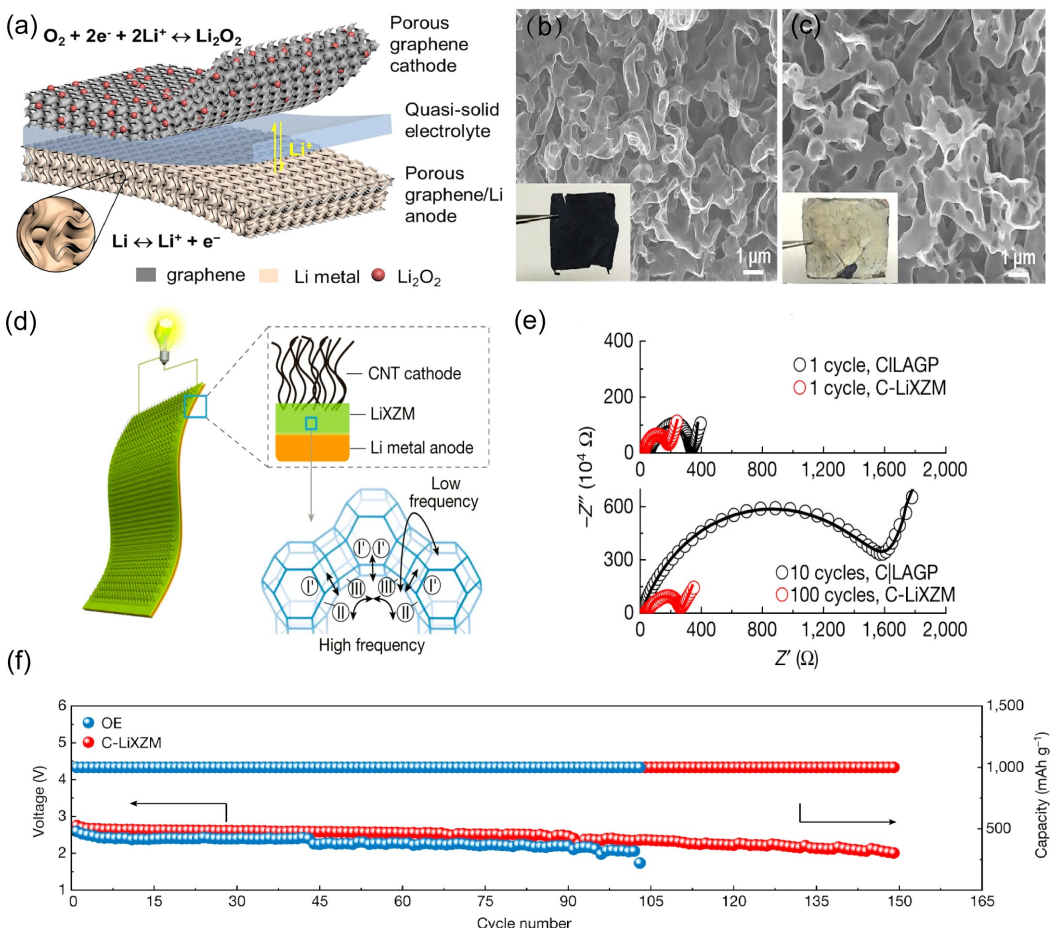


Figure 12. a) Configuration and components of quasi-solid-state rechargeable LOB. SEM images of b) porous graphene cathode and c) porous graphene/Li anode. Insets show the photographic images. Reprinted from Ref. [133] with permission. Copyright (2018) Springer Nature. d) Schematic of the integrated solid-state Li-air battery with C-LiXZM and the conduction mechanism of Li ions in LiX. e) EIS spectra of solid-state Li-air batteries with C-LiXZM and C|LAGP after different numbers of cycles. f) Terminal discharge voltage of batteries with the organic electrolyte and C-LiXZM at a current density of 500 mA g⁻¹ with the specific capacity limited to 1,000 mAh g⁻¹. Reprinted from Ref. [134] with permission. Copyright (2022) Springer Nature.

acceptable chemical and electrochemical stability, as it serves as the foundation of a solid-state battery. Presently, SSLOBs operate at low current density and limited power density due to internal resistance. This review briefly examines several possible SSEs. Although SPEs offer practical flexibility in LOBs, their application has been restricted by low Li⁺ conductivity at room temperature and insufficient mechanical strength. The use of GPEs, comprising a polymer matrix and an ionic liquid, has exhibited improved Li⁺ conductivity compared with SPEs. However, the liquid components of GPEs make them susceptible to particular battery-related issues. Furthermore, ionic liquid-based SSEs continue to dominate in terms of high Li⁺ conductivity, despite possessing significant interface contact resistance. Though combining several electrolytes to create CSEs is expected to offer synergistic benefits, it has yet to realize its maximum potential. Therefore, before realizing the commercial application of SSEs in LOBs, it is crucial to understand the ion-transport mechanisms and working mechanisms from a microscopic viewpoint. Consequently, further research is required to optimize existing electrolytes by incorporating different lithium salts, ionic liquids, crosslinking agents, and so

on. Additionally, accelerating the development of new SSEs remains an arduous task. Due to the increasing consumption of fossil fuels, large amounts of CO₂ are being emitted into the atmosphere, aggravating global climate change. Li–CO₂ batteries are attracting considerable attention as they provide practical and value-added opportunities for CO₂ conversion. Similar to LOBs, Li–CO₂ batteries also use organic LEs, which face risks of leakage. However, the electrochemical performance of current Li–CO₂ batteries is still inferior to that of LOBs. Therefore, the available work on SSEs in LOBs can serve as both a reference and an inspiration for developing stable SSEs in Li–CO₂ batteries.

Secondly, a well-designed multifunctional porous composite air cathode must remain stable under air/oxygen and oxygen radicals during the electrochemical reaction. For instance, an air cathode can utilize a non-carbon support layer on the surface of the carbon frame and RBC that can conduct both electrons and ions. Additionally, a continuous ion/electron transmission path between the cathode and SSEs is crucial for the reaction to occur in an active region. Currently, the common method is to create a composite electrode by mixing the positive active

material, SSE, and electronic conductor. Furthermore, the use of composite conductors can provide continuous and abundant TPBs by turning the point-to-point interface into a face-to-face interface. However, lithium dendrite growth and side reactions affect the efficiency and cycle life of the battery system, which hinders the application of Li metal anodes in solid-state batteries. Although recent research has focused on lithium dendrite, the mechanism of lithium dendrite growth on SSEs remains unclear. One hand, inserting a protective layer at the Li/SSE interface, such as an SEI film forming in situ on the surface of the Li metal anode or a functionalized diaphragm, is an effective way to block attacks of O₂, H₂O, and other elements. On the other hand, using Li mixed with other elements to form a Li-based alloy is conducive to rapid diffusion of Li and uniform Li deposition. Multilevel structure Li metal composites, which can promote interfacial Li⁺ transport and improve the interface contact with SSE, are worth exploring further.

Thirdly, current LOBs suffer from major shortcomings such as poor cycling stability, low round-trip efficiency, and overcharge potential during cycling, due to insufficient space for discharge products and inefficient removal of residues during recharge. To improve energy efficiency, an effective catalyst is urgently needed. Many solid catalysts have been used, including noble metals, transition metals, metal oxides, and metal carbides, to overcome this problem. In particular, integrating the air cathode, Li metal anode, and SSEs with traditional battery package methods, preparing the electrolyte layer, and then assembling the electrode layer on both sides may greatly improve battery performance. However, the battery's structure and assembly method could also substantially affect the actual performance of the battery. An ideal SSLOB with an integrated structure has been proposed, in which the SSE is integrated with cast Li as the anode and CNTs as the cathode via an in-situ assembly strategy. This approach could potentially result in higher practical energy density and long-term stability for the battery.

Finally, further research is needed to fully understand the underlying mechanisms of SSLOBs, including their working mechanism, ion transport mechanisms, Li deposition mechanism, and specific interfacial issues. Advanced characterization techniques, as well as a combination of laboratory experiments and related theoretical calculations, are crucial for gaining a better understanding of these systems. Given the ongoing developments and challenges facing SSLOBs, it is important to acknowledge that disruptive technologies do not happen overnight, but rather through continuous research and innovation, the future of SSLOBs looks bright.

Acknowledgements

This work was supported by NSFC (22279120 and 22202182) and Key R&D Projects in Henan Province (221111240100) in China.

Conflict of Interests

The authors declare no conflict of interest.

Keywords: Li–O₂ batteries • solid state electrolytes • solid polymer electrolytes • inorganic solid electrolytes • composite solid electrolytes

- [1] A. M. Omer, *Renewable Sustainable Energy Rev.* **2008**, *12*, 2265–2300.
- [2] C. Zhang, Y.-L. Wei, P.-F. Cao, M.-C. Lin, *Renewable Sustainable Energy Rev.* **2018**, *82*, 3091–3106.
- [3] M. Li, J. Lu, Z. Chen, K. Amine, *Adv. Mater.* **2018**, *30*, 1800561.
- [4] T.-H. Kim, J.-S. Park, S. K. Chang, S. Choi, J. H. Ryu, H.-K. Song, *Adv. Energy Mater.* **2012**, *2*, 860–872.
- [5] P. G. Bruce, S. A. Freunberger, L. J. Hardwick, J. M. Tarascon, *Nat. Mater.* **2011**, *11*, 19–29.
- [6] J. Lu, L. Li, J.-B. Park, Y.-K. Sun, F. Wu, K. Amine, *Chem. Rev.* **2014**, *114*, 5611–5640.
- [7] T. Liu, Z. Chang, Y. Yin, K. Chen, Y. Zhang, X. Zhang, *Solid State Ionics* **2018**, *318*, 88–94.
- [8] X. Yao, Q. Dong, Q. Cheng, D. Wang, *Angew. Chem. Int. Ed.* **2016**, *55*, 11344–11353.
- [9] K.-X. Wang, Q.-C. Zhu, J.-S. Chen, *Small* **2018**, *14*, 1800078.
- [10] Y. Liu, P. He, H. Zhou, *Adv. Energy Mater.* **2018**, *8*, 1701602.
- [11] I. Kowalczyk, J. Read, M. Salomon, *Pure Appl. Chem.* **2007**, *79*, 851–860.
- [12] L. Xu, G. Li, J. Guan, L. Wang, J. Chen, J. Zheng, *J. Energy Storage* **2019**, *24*, 100767.
- [13] L. Fan, S. Wei, S. Li, Q. Li, Y. Lu, *Adv. Energy Mater.* **2018**, *8*, 1702657.
- [14] X.-X. Wang, X.-W. Chi, M.-L. Li, D.-H. Guan, C.-L. Miao, J.-J. Xu, *Chem* **2023**, *9*, 394–410.
- [15] K. Funke, *Sci. Technol. Adv. Mater.* **2013**, *14*, 043502.
- [16] X. Zeng, M. Li, D. Abd El-Hady, W. Alshitari, A. S. Al-Bogami, J. Lu, K. Amine, *Adv. Energy Mater.* **2019**, *9*, 1900161.
- [17] K. M. Abraham, Z. Jiang, *J. Electrochem. Soc.* **1996**, *143*, 1–5.
- [18] H. Kitaura, H. Zhou, *Energy Environ. Sci.* **2012**, *5*, 9077–9084.
- [19] A. Paolella, W. Zhu, G.-L. Xu, A. La Monaca, S. Savoie, G. Girard, A. Vijh, H. Demers, A. Perea, N. Delaporte, A. Guerfi, X. Liu, Y. Ren, C.-J. Sun, J. Lu, K. Amine, K. Zaghib, *Adv. Energy Mater.* **2020**, *10*, 2001497.
- [20] C. Zhu, Q. Sun, J. Xie, Y. Jin, K. Wang, Z. Chen, J. Tu, G. Cao, X. Zhao, *New J. Chem.* **2018**, *42*, 19521–19527.
- [21] O. Sheng, C. Jin, X. Ding, T. Liu, Y. Wan, Y. Liu, J. Nai, Y. Wang, C. Liu, X. Tao, *Adv. Funct. Mater.* **2021**, *31*, 2100891.
- [22] a) H.-D. Lim, B. Lee, Y. Bae, H. Park, Y. Ko, H. Kim, J. Kim, K. Kang, *Chem. Soc. Rev.* **2017**, *46*, 2873–2888; b) B. Zhang, R. Tan, L. Yang, J. Zheng, K. Zhang, S. Mo, Z. Lin, F. Pan, *Energy Storage Mater.* **2018**, *10*, 139–159.
- [23] R. Chen, W. Qu, X. Guo, L. Li, F. Wu, *Mater. Horiz.* **2016**, *3*, 487–516.
- [24] M. Jaipal Reddy, T. Sreekanth, U. V. Subba Rao, *Solid State Ionics* **1999**, *126*, 55–63.
- [25] M. Forsyth, L. Porcarelli, X. Wang, N. Goujon, D. Mecerreyes, *Acc. Chem. Res.* **2019**, *52*, 686–694.
- [26] S. B. Aziz, T. J. Woo, M. F. Z. Kadir, H. M. Ahmed, *J. Sci. Adv. Mater. Devices* **2018**, *3*, 1–17.
- [27] J. Hassoun, F. Croce, M. Armand, B. Scrosati, *Angew. Chem.* **2011**, *123*, 3055–3058.
- [28] Z.-H. Huang, J. Li, L.-X. Li, H.-M. Xu, C. Han, M.-Q. Liu, J. Xiang, X.-Q. Shen, M.-X. Jing, *Ceram. Int.* **2022**, *48*, 25949–25957.
- [29] Y. Wu, Y. Li, Y. Wang, Q. Liu, Q. Chen, M. Chen, *J. Energy Chem.* **2022**, *64*, 62–84.
- [30] I. S. Noor, S. R. Majid, A. K. Arof, *Electrochim. Acta* **2013**, *102*, 149–160.
- [31] X. Liu, X. Xin, L. Shen, Z. Gu, J. Wu, X. Yao, *ACS Appl. Energ. Mater.* **2021**, *4*, 3975–3982.
- [32] M. Balaish, E. Peled, D. Golodnitsky, Y. Ein-Eli, *Angew. Chem.* **2015**, *127*, 446–450.
- [33] V. Viswanathan, K. S. Thygesen, J. S. Hummelshøj, J. K. Nørskov, G. Girishkumar, B. D. McCloskey, A. C. Luntz, *J. Chem. Phys.* **2011**, *135*, 214704.
- [34] a) C. Fanggao, G. A. Saunders, E. F. Lambson, R. N. Hampton, G. Carini, G. Di Marco, M. Lanza, *J. Poly. Sci. B Poly. Phys.* **1996**, *34*, 425–433; b) C. Zhao, L. Liu, X. Qi, Y. Lu, F. Wu, J. Zhao, Y. Yu, Y.-S. Hu, L. Chen, *Adv. Energy Mater.* **2018**, *8*, 1703012.
- [35] M. Balaish, M. Leskes, Y. Ein-Eli, *ACS Appl. Energ. Mater.* **2018**, *1*, 3048–3056.

- [36] W. Yu, C. Xue, B. Hu, B. Xu, L. Li, C.-W. Nan, *Energy Storage Mater.* **2020**, 27, 244–251.
- [37] M. Celik, A. Kizilaslan, M. Can, T. Cetinkaya, H. Akbulut, *Electrochim. Acta* **2021**, 371, 137824.
- [38] J. Yi, S. Guo, P. He, H. Zhou, *Energy Environ. Sci.* **2017**, 10, 860–884.
- [39] N. H. Idris, M. M. Rahman, J.-Z. Wang, H.-K. Liu, *J. Power Sources* **2012**, 201, 294–300.
- [40] A. Sarnowska, I. Polska, L. Niedzicki, M. Marcinek, A. Zalewska, *Electrochim. Acta* **2011**, 57, 180–186.
- [41] L. Long, S. Wang, M. Xiao, Y. Meng, *J. Mater. Chem. A* **2016**, 4, 10038–10069.
- [42] M. Walkowiak, A. Zalewska, T. Jesionowski, M. Pokora, *J. Power Sources* **2007**, 173, 721–728.
- [43] K. Liu, H. Sun, S. Dong, C. Lu, Y. Li, J. Cheng, J. Zhang, X. Wang, X. Chen, G. Cui, *Adv. Mater. Interfaces* **2017**, 4, 1700693.
- [44] S. M. Cho, J. Shim, S. H. Cho, J. Kim, B. D. Son, J. C. Lee, W. Y. Yoon, *ACS Appl. Mater. Interfaces* **2018**, 10, 15634–15641.
- [45] X. Zou, Q. Lu, Y. Zhong, K. Liao, W. Zhou, Z. Shao, *Small* **2018**, 14, 1801798.
- [46] D. Zhou, R. Liu, Y.-B. He, F. Li, M. Liu, B. Li, Q.-H. Yang, Q. Cai, F. Kang, *Adv. Energy Mater.* **2016**, 6, 1502214.
- [47] C. Zhao, J. Liang, Y. Zhao, J. Luo, Q. Sun, Y. Liu, X. Lin, X. Yang, H. Huang, L. Zhang, S. Zhao, S. Lu, X. Sun, *J. Mater. Chem. A* **2019**, 7, 24947–24952.
- [48] A. J. D'Angelo, M. J. Panzer, *Chem. Mater.* **2019**, 31, 2913–2922.
- [49] T. Yang, C. Shu, R. Zheng, M. Li, Z. Hou, P. Hei, Q. Zhang, D. Mei, J. Long, *ACS Sustainable Chem. Eng.* **2019**, 7, 17362–17371.
- [50] M. Ren, J. Zhang, C. Zhang, M. G. Stanford, Y. Chyan, Y. Yao, J. M. Tour, *ACS Appl. Energ. Mater.* **2020**, 3, 1702–1709.
- [51] P. Knauth, *Solid State Ionics* **2009**, 180, 911–916.
- [52] J. C. Bachman, S. Muy, A. Grimaud, H.-H. Chang, N. Pour, S. F. Lux, O. Paschos, F. Maglia, S. Lupart, P. Lamp, L. Giordano, Y. Shao-Horn, *Chem. Rev.* **2016**, 116, 140–162.
- [53] a) A. Manthiram, X. Yu, S. Wang, *Nat. Rev. Mater.* **2017**, 2, 16103; b) J. C. Bachman, S. Muy, A. Grimaud, H. H. Chang, N. Pour, S. F. Lux, O. Paschos, F. Maglia, S. Lupart, P. Lamp, L. Giordano, Y. Shao-Horn, *Chem. Rev.* **2016**, 116, 140–162.
- [54] Y. Huang, L. Zhao, L. Li, M. Xie, F. Wu, R. Chen, *Adv. Mater.* **2019**, 31, 1808393.
- [55] J. Wen, Y. Huang, J. Duan, Y. Wu, W. Luo, L. Zhou, C. Hu, L. Huang, X. Zheng, W. Yang, Z. Wen, Y. Huang, *ACS Nano* **2019**, 13, 14549–14556.
- [56] Y. Nikodimos, C.-J. Huang, B. W. Taklu, W.-N. Su, B. J. Hwang, *Energy Environ. Sci.* **2022**, 15, 991–1033.
- [57] A. Kondori, M. Esmaeilirad, A. M. Harzandi, R. Amine, M. T. Saray, L. Yu, T. Liu, J. Wen, N. Shan, H.-H. Wang, A. T. Ngo, P. C. Redfern, C. S. Johnson, K. Amine, R. Shahbazian-Yassar, L. A. Curtiss, M. Asadi, *Science* **2023**, 379, 499–505.
- [58] A. R. Symington, M. Molinari, J. A. Dawson, J. M. Statham, J. Purton, P. Canepa, S. C. Parker, *J. Mater. Chem. A* **2021**, 9, 6487–6498.
- [59] H. T. T. Le, D. T. Ngo, P. N. Didwal, J. G. Fisher, C.-N. Park, I.-D. Kim, C.-J. Park, *J. Mater. Chem. A* **2019**, 7, 3150–3160.
- [60] a) H. Aono, E. Sugimoto, Y. Sadaoka, N. Imanaka, G. y Adachi, *J. Electrochem. Soc.* **1990**, 137, 1023; b) H. Aono, E. Sugimoto, Y. Sadaoka, N. Imanaka, G.-y. Adachi, *B. Chem. Soc. Jpn.* **1992**, 65, 2200–2204.
- [61] C. J. Leo, G. V. Subba Rao, B. V. R. Chowdari, *Solid State Ionics* **2003**, 159, 357–367.
- [62] H. S. Jadhav, R. S. Kalubarme, S. Y. Jang, K. N. Jung, K. H. Shin, C. J. Park, *Dalton Trans.* **2014**, 43, 11723–11727.
- [63] H. S. Jadhav, R. S. Kalubarme, A. H. Jadhav, J. G. Seo, *Electrochim. Acta* **2016**, 199, 126–132.
- [64] T. Zhang, H. Zhou, *Nat. Commun.* **2013**, 4, 1817–1823.
- [65] X. Wang, D. Zhu, M. Song, S. Cai, L. Zhang, Y. Chen, *ACS Appl. Mater. Interfaces* **2014**, 6, 11204–11210.
- [66] Y.-P. Zhang, Y.-Q. Li, Z.-H. Cui, J.-C. Wang, O. Yamamoto, N. Imanishi, T. Zhang, *Sustain. Energy Fuels* **2020**, 4, 1600–1606.
- [67] X. Shen, Q. Zhang, T. Ning, T. Liu, Y. Luo, X. He, Z. Luo, A. Lu, *Mater. Today Chem.* **2020**, 18, 100368.
- [68] Y. Xing, N. Chen, M. Luo, Y. Sun, Y. Yang, J. Qian, L. Li, S. Guo, R. Chen, F. Wu, *Energy Storage Mater.* **2020**, 24, 707–713.
- [69] K.-N. Gao, H.-R. Wang, M.-H. He, Y.-Q. Li, Z.-H. Cui, Y. Mao, T. Zhang, *J. Power Sources* **2020**, 463, 228179.
- [70] Y. Xiao, K. Turcheniuk, A. Narla, A.-Y. Song, X. Ren, A. Magasinski, A. Jain, S. Huang, H. Lee, G. Yushin, *Nat. Mater.* **2021**, 20, 984–990.
- [71] G. Karkera, A. S. Prakash, *ACS Appl. Energ. Mater.* **2018**, 1, 1381–1388.
- [72] a) F. Croce, G. B. Appetecchi, L. Persi, B. Scrosati, *Nature* **1998**, 394, 456–458; b) W. Liu, S. W. Lee, D. Lin, F. Shi, S. Wang, A. D. Sendek, Y. Cui, *Nat. Energy* **2017**, 2, 17035; c) C.-L. Li, G. Huang, Y. Yu, Q. Xiong, J.-M. Yan, X.-B. Zhang, *Small* **2022**, 18, 2107833.
- [73] J. Yi, H. Zhou, *ChemSusChem* **2016**, 9, 2391–2396.
- [74] J.-B. Park, J. Hassoun, H.-G. Jung, H.-S. Kim, C. S. Yoon, I.-H. Oh, B. Scrosati, Y.-K. Sun, *Nano Lett.* **2013**, 13, 2971–2975.
- [75] J. Yi, Y. Liu, Y. Qiao, P. He, H. Zhou, *ACS Energy Lett.* **2017**, 2, 1378–1384.
- [76] Z. Gu, X. Xin, J. Yang, D. Guo, S. Yang, J. Wu, Y. Sun, X. Yao, *ACS Appl. Energ. Mater.* **2022**, 5, 9149–9157.
- [77] H. Chung, B. Kang, *Chem. Mater.* **2017**, 29, 8611–8619.
- [78] J. Wang, G. Huang, J. M. Yan, J. L. Ma, T. Liu, M. M. Shi, Y. Yu, M. M. Zhang, J. L. Tang, X. B. Zhang, *Natl. Sci. Rev.* **2021**, 8, nwaa150.
- [79] H. T. Le, D. T. Ngo, R. S. Kalubarme, G. Cao, C. N. Park, C. J. Park, *ACS Appl. Mater. Interfaces* **2016**, 8, 20710–20719.
- [80] S. Song, X. Qin, Y. Ruan, W. Li, Y. Xu, D. Zhang, J. Thokchom, *J. Power Sources* **2020**, 461, 228146.
- [81] S. Wang, J. Hu, X. Gui, S. Lin, Y. Tu, *J. Electrochem. Soc.* **2021**, 168, 020514.
- [82] C. Zhao, Q. Sun, J. Luo, J. Liang, Y. Liu, L. Zhang, J. Wang, S. Deng, X. Lin, X. Yang, H. Huang, S. Zhao, L. Zhang, S. Lu, X. Sun, *Chem. Mater.* **2020**, 32, 10113–10119.
- [83] J. Wang, Y. Yin, T. Liu, X. Yang, Z. Chang, X. Zhang, *Nano Res.* **2018**, 11, 3434–3441.
- [84] K. N. Jung, J. I. Lee, J. H. Jung, K. H. Shin, J. W. Lee, *Chem. Commun.* **2014**, 50, 5458–5461.
- [85] Z. Man, H. Tian, X. Zhu, Y. Wang, Y. Wu, X. Wen, Z. Lü, *J. Electrochem. Soc.* **2022**, 169, 060507.
- [86] Q. Wang, B. Liu, Y. Shen, J. Wu, Z. Zhao, C. Zhong, W. Hu, *Adv. Sci.* **2021**, 8, 2101111.
- [87] J. Bao, C. Li, F. Zhang, P. Wang, X. Zhang, P. He, H. Zhou, *Batteries & Supercaps* **2020**, 3, 708–712.
- [88] a) M. N. Obrovac, V. L. Chevrier, *Chem. Rev.* **2014**, 114, 11444–11502; b) G. He, Q. Li, Y. Shen, Y. Ding, *Angew. Chem.* **2019**, 131, 18637–18641.
- [89] S. Wu, J. Yi, K. Zhu, S. Bai, Y. Liu, Y. Qiao, M. Ishida, H. Zhou, *Adv. Energy Mater.* **2017**, 7, 1601759.
- [90] S. S. Zhang, D. Foster, J. Read, *J. Power Sources* **2010**, 195, 1235–1240.
- [91] B. D. McCloskey, A. Speidel, R. Scheffler, D. C. Miller, V. Viswanathan, J. S. Hummelshøj, J. K. Nørskov, A. C. Luntz, *J. Phys. Chem. Lett.* **2012**, 3, 997–1001.
- [92] a) R. E. Williford, J.-G. Zhang, *J. Power Sources* **2009**, 194, 1164–1170; b) S. B. Ma, D. J. Lee, V. Roev, D. Im, S.-G. Doo, *J. Power Sources* **2013**, 244, 494–498; c) M. D. Radin, D. J. Siegel, *Energy Environ. Sci.* **2013**, 6, 2370–2379.
- [93] L. Grande, E. Paillard, J. Hassoun, J.-B. Park, Y.-J. Lee, Y.-K. Sun, S. Passerini, B. Scrosati, *Adv. Mater.* **2015**, 27, 784–800.
- [94] a) M. M. Ottakam Thottil, S. A. Freunberger, Z. Peng, Y. Chen, Z. Liu, P. G. Bruce, *Nat. Mater.* **2013**, 12, 1050–1056; b) Z. Peng, S. A. Freunberger, Y. Chen, P. G. Bruce, *Science* **2012**, 337, 563–566.
- [95] S. Pakseresht, A. W. M. Al-Ogaili, T. Cetinkaya, M. Celik, H. Akbulut, *J. Power Sources* **2021**, 509, 230374.
- [96] M. Kim, H. Lee, H. J. Kwon, S.-M. Bak, C. Jaye, D. A. Fischer, G. Yoon, J. O. Park, D.-H. Seo, S. B. Ma, D. Im, *Sci. Adv.* **2022**, 8, eabm8584.
- [97] X. B. Zhu, T. S. Zhao, Z. H. Wei, P. Tan, L. An, *Energy Environ. Sci.* **2015**, 8, 3745–3754.
- [98] W. Zhang, Y. Shen, D. Sun, Z. Huang, Y. Huang, *Adv. Energy Mater.* **2017**, 7, 1602938.
- [99] X. Wang, S. Cai, D. Zhu, S. Mu, Y. Chen, *J. Solid State Electrochem.* **2015**, 19, 2421–2429.
- [100] X. B. Cheng, M. Q. Zhao, C. Chen, A. Pentecost, K. Maleski, T. Mathis, X. Q. Zhang, Q. Zhang, J. Jiang, Y. Gogotsi, *Nat. Commun.* **2017**, 8, 336–344.
- [101] J. Liu, M. Yue, S. Wang, Y. Zhao, J. Zhang, *Adv. Funct. Mater.* **2022**, 32, 2107769.
- [102] R. Xu, X.-B. Cheng, C. Yan, X.-Q. Zhang, Y. Xiao, C.-Z. Zhao, J.-Q. Huang, Q. Zhang, *Matter* **2019**, 1, 317–344.
- [103] H.-S. Lim, W.-J. Kwak, S. Chae, S. Wi, L. Li, J. Hu, J. Tao, C. Wang, W. Xu, J.-G. Zhang, *ACS Energy Lett.* **2021**, 6, 3321–3331.
- [104] Y. Sun, C. Zhao, K. R. Adair, Y. Zhao, L. V. Goncharova, J. Liang, C. Wang, J. Li, R. Li, M. Cai, T.-K. Sham, X. Sun, *Energy Environ. Sci.* **2021**, 14, 4085–4094.
- [105] J. Xiang, L. Yuan, Y. Shen, Z. Cheng, K. Yuan, Z. Guo, Y. Zhang, X. Chen, Y. Huang, *Adv. Energy Mater.* **2018**, 8, 1802352.

- [106] Y. Sun, K. Chen, C. Zhang, H. Yu, X. Wang, D. Yang, J. Wang, G. Huang, S. Zhang, *Small* **2022**, *18*, e2201470.
- [107] T. N. Hsia, H. C. Lu, Y. C. Hsueh, S. Rajesh Kumar, C. S. Yen, C. C. Yang, S. Jessie Lue, *J. Colloid Interface Sci.* **2022**, *626*, 524–534.
- [108] Y. Sun, M. Amirmaleki, Y. Zhao, C. Zhao, J. Liang, C. Wang, K. R. Adair, J. Li, T. Cui, G. Wang, R. Li, T. Filleter, M. Cai, T. K. Sham, X. Sun, *Adv. Energy Mater.* **2020**, *10*, 2001139.
- [109] T. Liu, X. L. Feng, X. Jin, M. Z. Shao, Y. T. Su, Y. Zhang, X. B. Zhang, *Angew. Chem.* **2019**, *131*, 18408–18413.
- [110] C. Zhao, J. Liang, Q. Sun, J. Luo, Y. Liu, X. Lin, Y. Zhao, H. Yadegari, M. N. Banis, R. Li, H. Huang, L. Zhang, R. Yang, S. Lu, X. Sun, *Small Methods* **2019**, *3*, 1800437.
- [111] Q. Wu, L. Yang, X. Wang, Z. Hu, *Sci. China Chem.* **2020**, *63*, 665–681.
- [112] C. Li, Y. Liu, B. Li, F. Zhang, Z. Cheng, P. He, H. Zhou, *Nanotechnology* **2019**, *30*, 364003.
- [113] X. Zhu, T. Zhao, P. Tan, Z. Wei, M. Wu, *Nano Energy* **2016**, *26*, 565–576.
- [114] L. Xiao, E.-W. Li, J.-Y. Yi, W. Meng, B.-H. Deng, J.-P. Liu, *Rare Met.* **2018**, *37*, 527–535.
- [115] S. Song, D. Zhang, Y. Ruan, L. Yu, Y. Xu, J. Thokchom, D. Mei, *ACS Appl. Energ. Mater.* **2021**, *4*, 6221–6232.
- [116] C. L. Li, G. Huang, Y. Yu, Q. Xiong, J. M. Yan, X. B. Zhang, *Small* **2022**, *18*, e2107833.
- [117] J. Wang, G. Huang, K. Chen, X. B. Zhang, *Angew. Chem. Int. Ed.* **2020**, *59*, 9382–9387.
- [118] Y. Lu, Y. Cai, Q. Zhang, L. Liu, Z. Niu, J. Chen, *Chem. Sci.* **2019**, *10*, 4306–4312.
- [119] X. Zhu, Z. Chang, H. Yang, P. He, H. Zhou, *J. Mater. Chem. A* **2022**, *10*, 651–663.
- [120] C. Zhao, Y. Zhu, Q. Sun, C. Wang, J. Luo, X. Lin, X. Yang, Y. Zhao, R. Li, S. Zhao, H. Huang, L. Zhang, S. Lu, M. Gu, X. Sun, *Angew. Chem.* **2021**, *133*, 5885–5890.
- [121] N. Feng, P. He, H. Zhou, *ChemSusChem* **2015**, *8*, 600–602.
- [122] T. Liu, M. Leskes, W. Yu, A. J. Moore, L. Zhou, P. M. Bayley, G. Kim, C. P. Grey, *Science* **2015**, *350*, 530–533.
- [123] W.-J. Kwak, D. Hirshberg, D. Sharon, M. Afri, A. A. Frimer, H.-G. Jung, D. Aurbach, Y.-K. Sun, *Energy Environ. Sci.* **2016**, *9*, 2334–2345.
- [124] a) S. Matsuda, Y. Kubo, K. Uosaki, K. Hashimoto, S. Nakanishi, *J. Phys. Chem. C* **2016**, *120*, 13360–13365; b) Q. Zhang, Y. Zhou, W. Dai, X. Cui, Z. Lyu, Z. Hu, W. Chen, *Batteries & Supercaps* **2021**, *4*, 232–239.
- [125] A. Ahmadiparidari, S. Fuladi, L. Majidi, S. Plunkett, E. Sarnello, H. Gholivand, Z. Hemmat, S. Rastegar, S. N. Misal, N. Jimenez, P. C. Redfern, J. Wen, T. Li, A. T. Ngo, F. Khalili-Araghi, L. A. Curtiss, A. Salehi-Khojin, *J. Power Sources* **2021**, *491*, 229506.
- [126] Y. Chen, S. A. Freunberger, Z. Peng, O. Fontaine, P. G. Bruce, *Nat. Chem.* **2013**, *5*, 489–494.
- [127] B. J. Bergner, A. Schürmann, K. Peppler, A. Garsuch, J. Janek, *J. Am. Chem. Soc.* **2014**, *136*, 15054–15064.
- [128] S. H. Lee, J.-B. Park, H.-S. Lim, Y.-K. Sun, *Adv. Energy Mater.* **2017**, *7*, 1602417.
- [129] L. Shi, G. Wang, J. Li, M. Wu, Z. Wen, *ACS Sustainable Chem. Eng.* **2021**, *9*, 13883–13892.
- [130] Y. Hou, L. Jiang, Y. Zhang, Z. Qin, C. Jiang, M. Wang, *Chin. J. Chem. Eng.* **2021**, *34*, 208–216.
- [131] F. Sultana, K. Althubeiti, K. M. Abualnaja, J. Wang, A. Zaman, A. Ali, S. A. Arbab, S. Uddin, Q. Yang, *Dalton Trans.* **2021**, *50*, 16386–16394.
- [132] M. Ren, J. Chen, G. Wu, E. A. McHugh, A.-L. Tsai, J. M. Tour, *ACS Catal.* **2021**, *11*, 1833–1840.
- [133] G. Huang, J. Han, C. Yang, Z. Wang, T. Fujita, A. Hirata, M. Chen, *NPG Asia Mater.* **2018**, *10*, 1037–1045.
- [134] X. Chi, M. Li, J. Di, P. Bai, L. Song, X. Wang, F. Li, S. Liang, J. Xu, J. Yu, *Nature* **2021**, *592*, 551–557.

Manuscript received: May 31, 2023

Revised manuscript received: July 27, 2023

Accepted manuscript online: July 28, 2023

Version of record online: August 24, 2023